nature materials

ARTICLES

https://doi.org/10.1038/s41563-020-0615-x

Check for updates

Reprogramming normal cells into tumour precursors requires ECM stiffness and oncogene-mediated changes of cell mechanical properties

Tito Panciera[1,10], Anna Citron[1,10], Daniele Di Biagio[1], Giusy Battilana[1], Alessandro Gandin[2], Stefano Giulitti[1], Mattia Forcato[3], Silvio Bicciato[3], Valeria Panzetta[4,5], Sabato Fusco[4,5], Luca Azzolin[1], Antonio Totaro[1], Angelo Paolo Dei Tos[6], Matteo Fassan[6], Vincenzo Vindigni[7], Franco Bassetto[7], Antonio Rosato[8], Giovanna Brusatin[2], Michelangelo Cordenonsi[1]✉ and Stefano Piccolo[1,9]✉

Defining the interplay between the genetic events and microenvironmental contexts necessary to initiate tumorigenesis in normal cells is a central endeavour in cancer biology. We found that receptor tyrosine kinase (RTK)–Ras oncogenes reprogram normal, freshly explanted primary mouse and human cells into tumour precursors, in a process requiring increased force transmission between oncogene-expressing cells and their surrounding extracellular matrix. Microenvironments approximating the normal softness of healthy tissues, or blunting cellular mechanotransduction, prevent oncogene-mediated cell reprogramming and tumour emergence. However, RTK–Ras oncogenes empower a disproportional cellular response to the mechanical properties of the cell's environment, such that when cells experience even subtle supra-physiological extracellular-matrix rigidity they are converted into tumour-initiating cells. These regulations rely on YAP/TAZ mechanotransduction, and YAP/TAZ target genes account for a large fraction of the transcriptional responses downstream of oncogenic signalling. This work lays the groundwork for exploiting oncogenic mechanosignalling as a vulnerability at the onset of tumorigenesis, including tumour prevention strategies.

The minimal compendium of genetic and epigenetic changes sufficient to turn a normal cell into a tumorigenic one remains a central unanswered question in cancer biology. Normal tissues have recently been shown to carry clones of healthy cells bearing a host of oncogenic alterations[1–3]. Thus, oncogenes appear insufficient to drive tumour initiation in living tissues, consistent with the view that cancer is not just a genetic disease, but rather is the product of an aberrant communication between the cell and its microenvironment.

In this vein, the mechanical signals that the cell receives from its surroundings are emerging as overarching determinants of its behaviour[4,5] and are known to foster tumour progression[6]. What remains unexplored is the role of altered cell mechanics in the pivotal preceding step—that is, the reprogramming of normal cells into cells endowed with tumorigenic properties. Here we explore whether and how common genetic drivers of tumorigenesis can reprogram normal cells into tumour-precursor cells (a process hereafter referred to as oncogenic reprogramming) by establishing an interplay between the physical attributes of cells and their microenvironment at the beginning of tumorigenesis. We focused on the RTK–Ras cascade because of its widespread relevance for human cancer[7].

Results

Mechanical signalling is required for the transformation of primary cells. As first paradigm, we focused on mammary gland tumorigenesis. Mammary tumours emerge from luminal cells that have acquired a self-renewing potential and ability to seed tumours when transplanted into an immunocompromised host[8]. RTK–Ras signalling is a potent driver of mammary tumorigenesis due to the overexpression of growth factor receptors, such as HER2, EGFR or FGFR. We first tested whether freshly explanted luminal differentiated (LD) cells from healthy mouse and human mammary glands, normally void of any proliferative potential[9,10], can be reprogrammed into cells able to proliferate and self-renew by the expression of a constitutively active form of HER2 (HER2-CA). LD cells purified by fluorescence-activated cell sorting (FACS; see Methods) were plated on collagen-coated dishes and transduced with lentiviral vectors encoding either EGFP or the activated version of HER2 (see schemes in Extended Data Fig. 1a,c). Remarkably, oncogenic signalling conferred to mouse and human LD cells the ability to form self-renewing colonies (Fig. 1a–d) that developed into solid organoids entirely composed of K8$^+$ luminal cells, a hallmark of human HER2$^+$ breast cancer (Fig. 1e).

[1]Department of Molecular Medicine, University of Padua School of Medicine, Padua, Italy. [2]Department of Industrial Engineering and INSTM, University of Padua, Padua, Italy. [3]Center for Genome Research, Department of Life Sciences, University of Modena and Reggio Emilia, Modena, Italy. [4]Interdisciplinary Research Centre on Biomaterials, CRIB, University of Naples Federico II, Naples, Italy. [5]Center for Advanced Biomaterials for Health Care IIT@CRIB, Istituto Italiano di Tecnologia, Naples, Italy. [6]Department of Medicine (DIMED), Surgical Pathology and Cytopathology Unit, Padua, Italy. [7]Clinic of Plastic Surgery, Padua University Hospital, Padua, Italy. [8]Istituto Oncologico Veneto IOV-IRCCS, and Department of Surgery, Oncology and Gastroenterology, University of Padua School of Medicine, Padua, Italy. [9]IFOM, The FIRC Institute of Molecular Oncology, Padua, Italy. [10]These authors contributed equally: Tito Panciera, Anna Citron. ✉e-mail: michelangelo.cordenonsi@unipd.it; piccolo@bio.unipd.it

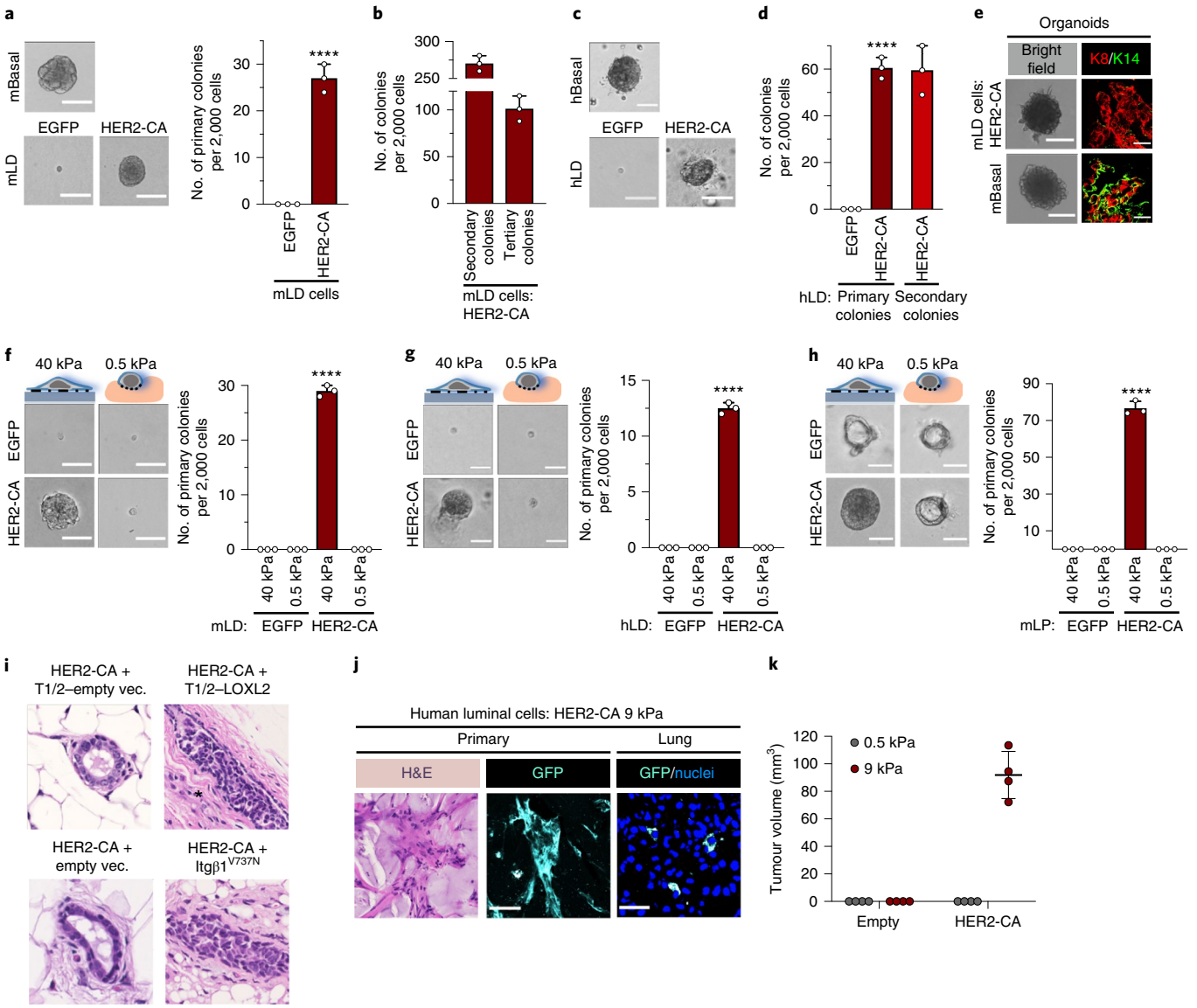

Fig. 1 | Abnormal substrate rigidity is required for oncogenes to reprogram normal mammary cells into tumorigenic ones. a,**b**, Representative images (**a**) and quantifications (**b**) of murine LD (mLD)-derived colonies. Murine basal cell (mBasal)-derived colonies are shown for comparison. Scale bars, 170 µm. $^{****}P = 9.9 \times 10^{-5}$. See also Extended Data Fig. 1b,e. **c**,**d**, Representative images (**c**) and quantifications (**d**) of colonies formed by human LD (hLD) cells. Colonies formed by human mammary basal cells (hBasal) are shown for comparison. Scale bars, 170 µm. $^{****}P = 2.0 \times 10^{-5}$. See also Extended Data Fig. 1d,f. **e**, Representative bright-field and immunofluorescence images ($n = 3$ independent experiments) of organoids formed by mLD cells expressing HER2-CA. Organoids formed by mBasal cells are shown for comparison. K14 and K8 serve as markers of basal and luminal cell identity, respectively. Scale bars, 400 µm (left) and 17 µm (right). **f**–**h**, Representative images and quantifications of solid colonies formed by mLD (**f**), hLD (**g**) or murine LP (mLP) (**h**) cells, cultured on 40 kPa or on 0.5 kPa hydrogels and then seeded in clonogenic medium. Scale bars, 170 µm. $^{****}P = 5.2 \times 10^{-12}$ (**f**),1.69×10^{-11} (**g**) and 1.68×10^{-12} (**h**). See also Extended Data Fig. 1g,h. **i**, Representative pictures ($n = 5$) of the in vivo outgrowths generated from mLD cells. T1/2, C3H10T1/2 fibroblasts; vec., vector. See Extended Data Fig. 1m, demonstrating increased fibrillar collagen organization by LOXL2. **j**, Representative haematoxylin and eosin (H&E) images ($n = 4$) of subcutaneous tumours and lung-disseminated GFP-traced tumour cells derived from indicated hLD cells. Scale bars, 80 µm for primary tumour and 25 µm for lung. **k**, Quantifications of the volume of subcutaneous outgrowths generated from control or the indicated reprogrammed hLDs injected within hydrogels of the indicated stiffness. Data are the mean ± s.d. of $n = 4$ independent experiments. In **a**, **b**, **d** and **f**–**h**, the data are the mean + s.d. of $n = 3$ biologically independent samples. *P* values were determined by the unpaired two-sided Student's *t*-test (**a**,**d**) or one-way ANOVA with Sidak's multiple-comparisons test (**f**–**h**).

To test the relevance of extracellular matrix (ECM) rigidity in HER2-driven oncogenic reprogramming, we repeated the above experiment but plated primary cells on soft adhesive hydrogels of 0.5 kPa, phenocopying the compliance of the normal mammary gland[11]. Remarkably, oncogenic activation was unable to induce reprogramming of the cells experiencing these physiological levels of substrate stiffness (Fig. 1f,g), as these cells invariably remained differentiated single cells. Similar experiments were carried out using FACS-purified luminal progenitor (LP) cells. Upon plating in colony medium, LP cells formed cyst-like outgrowths that, as previously reported, lacked self-renewal potential[10]. As a control, when HER2-expressing LD or LP cells were plated on the same hydrogels,

but tuned to a higher rigidity (40 kPa), they were converted into proliferating cells that formed self-renewing solid colonies (Fig. 1f–h) and organoids composed of $K8^+$ cells (Extended Data Fig. 1i), a similar result to that observed above on tissue culture plastics (3 GPa). Thus, an appropriate mechanical environment is required for oncogenic reprogramming of primary cells.

Next, we aimed to establish whether mechanical inputs are also instrumental in vivo at reprogramming oncogene-expressing cells into cells endowed with tumorigenic properties. We tested this idea first in mouse and then in human primary luminal cells, using independent means to manipulate cell mechanics in vivo. First, HER2-expressing mouse LD cells were transplanted in the cleared mammary fat pad of immunocompromised mice, together with C3H10T1/2 fibroblasts expressing LOXL2, a secreted enzyme well known to increase ECM stiffness by promoting collagen cross-linking[12]. This combination was sufficient to induce tumour formation (ductal carcinoma in situ, DCIS; Fig. 1i and Extended Data Fig. 1j,k). Co-transplantation with control (empty-vector-expressing) C3H10T1/2 fibroblasts, however, was insufficient to induce any tumour formation, as co-transplanted HER2-expressing LD cells generated only short, monostratified luminal duct primordia (Fig. 1i and Extended Data Fig. 1j,k), similarly to HER2-expressing LD cells alone. Similar conclusions could be inferred from ex vivo experiments involving mammary organoid cultures expressing HER2 and treated with LOXL2 (Extended Data Fig. 1l).

As an independent procedure to demonstrate the relevance of mechanical signalling for oncogenic cell reprogramming, we co-expressed HER2-CA with $Itgb1^{V737N}$, a self-clustering integrinβ_1 mutant (encoded by *Itgb1*^{V737N}) that mimics, cell autonomously, the effect of a stiff ECM at adhesion sites[13]. This combination also induced DCIS formation, whereas LD cells expressing $Itgb1^{V737N}$ alone formed no outgrowth (Fig. 1i and Extended Data Fig. 1j,k,n).

Third, we used HER2-expressing and GFP-labelled primary human luminal cells and injected these into recipient mice embedded in either soft (0.5 kPa) or stiff (9 kPa) hyaluronic acid (HA)-based hydrogels. Palpable tumours could be detected after 7 weeks, only from HER2-CA-expressing cells embedded within the stiff HA-based hydrogel (Fig. 1j,k). By histological examination, these neoplastic lesions were found to be characterized by poor cellularity, massive ECM deposition and aggressiveness, with cells radiating out of the tumour centre through collective migration or as stretched tumour cells aligned to stromal fibres (Fig. 1j and Extended Data Fig. 1o). Immunostaining revealed the presence of individual human cells homed in the mouse lung, but in an ostensibly quiescent state (Fig. 1j). These results indicate that increased mechanical signalling from the microenvironment is crucial for oncogenes to initiate tumorigenesis, while the normal softness of healthy tissues averts oncogene function.

Oncogenes empower disproportional mechanical responsiveness. Our findings indicate that a dual requirement must be met for a normal cell to undergo oncogenic reprogramming: (1) a cell-autonomous event, that is, oncogenic activation, and (2) a non-cell-autonomous event, that is, increased stiffness of the environment. Are these distinct inputs or in fact feeding on the same pathway? The ability of a cell to respond to mechanical signals is intimately connected to the cell's ability to pull against the ECM, as determined by the tensional and architectural organization of the cytoskeleton[5,14,15]. We thus assessed the traction forces developed by non-tumorigenic immortalized mammary cells (MCF10A) induced to express $K\text{-}Ras^{G12V}$ or HER2-CA. We first measured the ability of these cells to contract a collagen gel in which they were embedded. We found that oncogenes greatly empower cell contractility (Fig. 2a). When assessed by traction force microscopy (TFM), cells expressing $K\text{-}Ras^{G12V}$ or HER2-CA applied significantly stronger traction stresses when compared with parental (empty-vector-transduced) cells (Fig. 2b). Consistent with this, transformed cells displayed increased contractile actomyosin bundles as visualized by increased levels of phosphorylated myosin light chain (pMLC; Fig. 2c and Extended Data Fig. 2b). Increased intracellular contractility also directly impacts the formation and maturation of focal adhesions (FAs)[16], and, in line with this, HER2- or K-Ras-expressing cells displayed increased FA formation and maturation (Extended Data Fig. 2c,d). YAP and TAZ are two highly related transcriptional regulators serving as well-established sensors of mechanotransduction[4,15]. We found that cell-autonomous changes in cell mechanics induced by oncogenes led to massive activation of YAP/TAZ, as visualized by their nuclear accumulation (Fig. 2d); YAP/TAZ binding to their DNA-binding platform TEAD (Extended Data Fig. 2e); and induction of YAP/TAZ-dependent transcriptional activity (Extended Data Fig. 2f,g). These data suggest that activated oncogenes increase cellular mechanoperception.

We then sought to determine whether oncogenes change the cell's mechanical properties and the dependency of this response on the substrate material properties. For this, we used multiple-particle-tracking microrheology, a procedure that probes the mechanical attributes of the F-actin cytoskeleton providing a global picture of the stiffness of an individual cell[17]. Control and oncogene-expressing cells remained equally soft when challenged at levels of ECM rigidity similar to those experienced by mammary cells within the healthy mammary gland (0.5 kPa; Fig. 2e). However, only oncogene-expressing cells were able to stiffen when challenged at a rigidity value (1 kPa) approaching those of mammary tumours[11], even if these stiffness values corresponded to an ostensibly modest change in the substrate's rheology when compared with normal mammary tissue (Fig. 2e). Thus, oncogenes should enable epithelial cells to biologically respond to mechanical stimuli that are otherwise sub-threshold for non-oncogene-expressing cells. Consistent with this, oncogenes specifically empowered the ability to engage YAP/TAZ activation at 1 kPa, but not at 0.5 kPa (Fig. 2f,g and Extended Data Fig. 2j).

Thus, cell contractility and microrheology assays support the view that oncogenic signalling disproportionally enhances cellular mechanotransduction in response to the physical inputs received from the environment. Oncogene activity alone is insufficient to reprogram normal cells in the absence of sufficiently matching, and mechanically empowering, extracellular rigidity. Reducing extracellular stiffness to the very compliant values seen for natural tissues inevitably decreases cell rigidity to levels that become impossible to compensate by RTK–Ras oncogenes, and this averts cell reprogramming towards a tumorigenic fate, as visualized in vivo (Fig. 1).

The above findings predict that even a relatively modest increase in the substrate rigidity of the microenvironment in which oncogene-expressing cells are embedded should be sufficient to ignite oncogenic mechanosignalling and empower oncogene-mediated cell reprogramming. To test this hypothesis and expand the generality of our conclusions, we focused on pancreatic tumorigenesis. Human pancreatic neoplasias are characterized by activating mutations in *KRAS* that occur at exceedingly high frequencies (>90%)[18], and this is recapitulated in mouse models, where Ras mutation is indeed a potent driver for pancreatic tumorigenesis[19]. That said, even in these cases, tumour emergence is extraordinarily rare if one considers that most cells remain normal and healthy throughout the mouse lifespan in spite of continuous expression of mutant K-Ras[19]. Thus, additional events ostensibly appear to be required to initiate tumorigenesis in pancreata expressing oncogenic Ras. The cell of origin of pancreatic cancer is the exocrine acinar cell that, after Ras activation, undergoes a change of fate known as acinar-to-ductal metaplasia (ADM), accompanied by the reactivation of cell proliferation[20]. This step can be recapitulated in ex vivo cultures by expression of activated $K\text{-}Ras^{G12D}$ in freshly explanted acini, which, after seeding in a 3D collagen I ECM, convert to self-expanding ductal organoids (see scheme of Extended Data Fig. 3a).

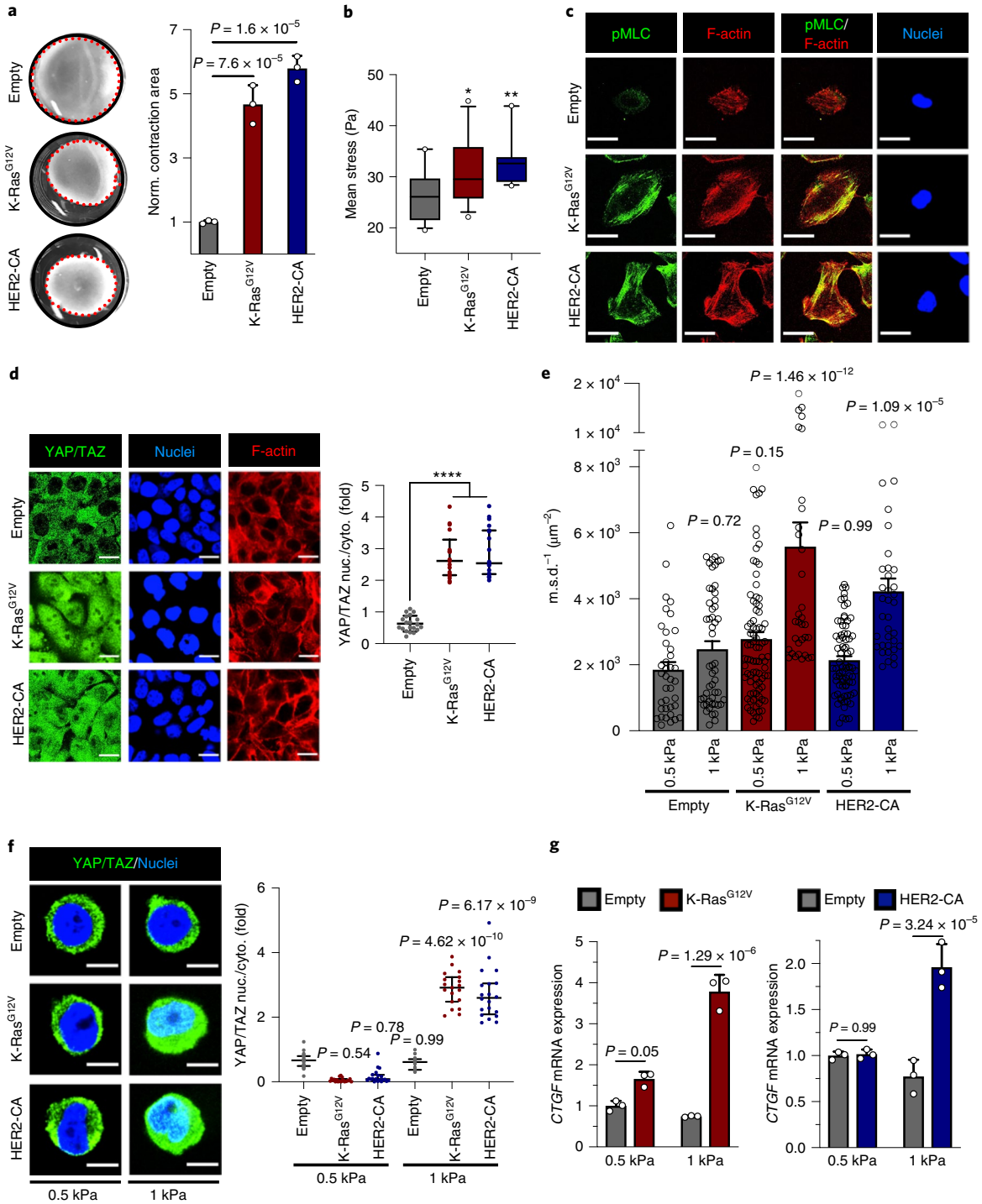

Fig. 2 | RTK–Ras oncogenes change the mechanical and material properties of cells. a, Representative images ($n = 3$) and normalized (Norm.) quantifications of collagen contraction assays performed with MCF10A cells. Data are mean + s.d. of $n = 3$ biologically independent samples. Empty, empty vector. See controls in Extended Data Fig. 2a. **b**, Traction force microscopy measurements of mean stresses exerted by the indicated MCF10A cells on 3 kPa substrates. Data are box-and-whiskers plots (whiskers: from 10th to 90th percentile; box: from 25th to 75th percentile; line within the box: median) of $n > 12$ independent samples. $^{**}P = 0.0034$, $^{*}P = 0.049$. **c**, Representative immunofluorescence images for pMLC of the indicated MCF10A cells. Scale bars, 24 µm. Images are representative of $n = 3$ independent experiments. Quantifications are in Extended Data Fig. 2b. **d**, Representative immunofluorescence images and quantifications of the nuclear-to-cytoplasmic (nuc./cyto.) subcellular localization of YAP/TAZ in post-confluent MCF10A cells. Scale bars, 16 µm. Data are mean ± s.d. of $n > 17$ independent samples. $^{****}P = 10^{-15}$. YAP/TAZ are downstream of oncogene-induced contractility (Extended Data Fig. 2h). **e**, Particle-tracking microrheology of the indicated MCF10A cells seeded on 0.5 kPa and 1 kPa hydrogels. Data are mean + s.d. of $n > 35$ biologically independent samples. **f**, Representative immunofluorescence images and quantifications of YAP/TAZ localization in single MCF10A cells on 0.5 and 1 kPa hydrogels. Scale bars, 8 µm. Data are mean ± s.d. of $n > 17$ independent samples. See also Extended Data Fig. 2i,k. **g**, Quantitative real-time PCRs (qRT-PCRs) assessing the expression levels of the YAP/TAZ endogenous target *CTGF* (also known as *CCN2*) in MCF10A cells seeded on 0.5 or 1 kPa hydrogels. Data are mean + s.d. of $n = 3$ biologically independent samples. *P* values were determined by the unpaired two-sided *t*-test (**a**,**b**) or one-way ANOVA with Sidak's multiple-comparisons test (**d**–**g**).

To test whether K-Ras^{G12D}-mediated cell reprogramming is blunted at physiological stiffness levels but promoted by quantal increases in substrate mechanics, we embedded K-Ras^{G12D}-expressing acini in distinct synthetic HA-based matrices offering comparable adhesivity but tuned at different rigidities[15,21] (see scheme in Extended Data Fig. 3b). K-Ras^{G12D} was insufficient to induce ADM at the lowest stiffness (0.1 kPa); however, K-Ras^{G12D}-expressing acini started to reprogram at intermediate rigidity levels (0.2 kPa) and all underwent ADM at higher rigidities (>0.5 kPa; Fig. 3a). By gene expression, K-Ras^{G12D}-expressing acini experiencing a stiffer ECM lost the expression of the differentiation marker amylase and acquired the expression of ductal/progenitor markers, such as K19 and Sox9, whereas K-Ras^{G12D}-expressing acini embedded in a soft ECM remained fully differentiated, indistinguishable from the control (Fig. 3b). As a readout of Ras-induced mechanosignalling in pancreatic acini, we monitored YAP/TAZ nuclear localization and found that oncogenic Ras induced YAP/TAZ activation at a permissive ECM rigidity but not in compliant conditions (Fig. 3c and Extended Data Fig. 3c). We conclude from these experiments that oncogenic signalling must be matched by sufficient ECM rigidity to promote the early step of pancreatic tumorigenesis.

Our model predicts that reducing cell mechanics by interfering with the cell tensional state should prevent oncogenic cell reprogramming. Indeed, K-Ras^{G12D}-expressing acini treated with inhibitors of focal adhesion kinase (FAK) or by using a low (vital) dose of the F-actin inhibitor cytochalasin-D (Cyto.D)[4] remained fully differentiated without any sign of ADM (Fig. 3d,e and Extended Data Fig. 3d); this correlated with failure to activate YAP/TAZ (Fig. 3d and Extended Data Fig. 3e).

In light of the above results, we asked whether tumour initiation in vivo could be prevented by blunting the mechanical interplay between oncogene-expressing cells and their substrate. We did so by lowering either ECM or intracellular mechanics. For this, we took advantage of mice conditionally expressing oncogenic K-Ras^{G12D} and mutant p53^{R172H} in adult pancreatic acini (*Ptf1a-cre^{ERTM}*; *Kras$^{LSL\text{-}G12D}$*; *Trp53$^{LSL\text{-}R172H}$*). After tamoxifen administration, these mice developed neoplasias (PanINs) at a high frequency (Fig. 3f and Extended Data Fig. 3h). Pancreatic cancer is known for being a very rigid tumour, and indeed, tumours generated from cells expressing K-Ras^{G12D} and p53^{R172H} were surrounded by a collagen-rich fibrous ECM and displayed elevated pMLC2 staining from the earliest stage of tumorigenesis (PanIN1; Fig. 3f and Extended Data Fig. 3i,j). Yet the role of altered cell mechanics in the early step of tumour emergence remains unclear. To attenuate ECM mechanics in vivo, mice expressing oncogenic Ras and mutant p53 in their acinar cells were treated with β-aminopropionitrile (BAPN), an inhibitor of the LOX family of collagen cross-linking enzymes (see scheme in Extended Data Fig. 3g). No neoplastic lesions whatsoever (that is, neither PanINs nor PDACs) developed in BAPN-treated pancreata (Fig. 3f and Extended Data Fig. 3h), with pancreatic parenchyma remaining ostensibly normal over the 11 weeks during which we monitored these mice. BAPN treatment inhibited the deposition of collagen fibres, normalized the cells' tensional state (Extended Data Fig. 3i,j) and prevented YAP/TAZ activation (Fig. 3f).

In complementary experiments, to inhibit intracellular mechanics, we treated Ras^{G12D}-expressing *Ptf1a-cre^{ERTM}*; *Kras$^{LSL\text{-}G12D}$* adult mice with fasudil, an FDA-approved drug that inhibits Rho-associated protein kinase (ROCK), a main orchestrator of actomyosin contractility (see scheme of Extended Data Fig. 3g). Similarly to BAPN-mediated tumour prevention, fasudil administration also abolished any emergence of neoplasia (Fig. 3g and Extended Data Fig. 3k). The massive nuclear accumulation of YAP/TAZ induced by oncogenic Ras was blunted by fasudil treatment, correlating with the normalization of cellular tension as visualized by pMLC (Fig. 3g and Extended Data Fig. 3l).

Oncogenic mechanosignalling mediated by YAP/TAZ. We next asked by what means changes in cell mechanical and material properties induced by oncogenes could convert normal cells into tumour-precursor cells. Clearly, this had to ultimately involve changes in the cell's transcriptome, and YAP/TAZ mechanotransduction as the mediator of these responses represented the most likely culprit[4]. Indeed, YAP and TAZ are essential mediators of tumour emergence in the mammary gland and pancreas[22,23], a finding also replicated in this study (Extended Data Fig. 4a,b). To test whether YAP and TAZ act as nuclear effectors of oncogenic mechanosignalling for primary cell reprogramming, we carried out YAP/TAZ knockout in explanted mammary LD or pancreatic acinar cells expressing oncogenes and challenged cells at ECM rigidities permissive for transformation. For this, we used primary cells explanted from mice bearing *loxP*-flanked YAP/TAZ alleles (*Yap$^{fl/fl}$*; *Taz$^{fl/fl}$*). Remarkably, we found that YAP and TAZ are genetically required to sustain HER2-induced reprogramming of primary mouse LD cells, and to sustain K-Ras-induced pancreatic reprogramming in organoids (Fig. 4a,b and Extended Data Fig. 4c). Crucially, by using cells explanted from doxycycline-inducible *tetO-Yap^{S127A}* transgenic mice, we also found that YAP overexpression could single-handedly rescue oncogene-induced pancreatic cell reprogramming in mechanical conditions otherwise prohibitory for oncogene function (Fig. 4c,d and Extended Data Fig. 4e,g).

Finally, we aimed to determine, unbiasedly and at the genome-wide level, to what extent YAP/TAZ-dependent transcription serves as a mediator of oncogene-induced mechanosignalling. For this, we compared by RNA-seq the transcriptome of control and YAP/TAZ-depleted HER2-CA-expressing immortalized mammary cells experiencing two extreme rigidities: (1) stiff, fibronectin-coated tissue culture dishes (a paradigm of standard tissue culture conditions) and (2) a fibronectin-coated soft substrate (0.5 kPa; Fig. 4e). The hierarchical clustering of HER2-CA-induced genes showed that the transcriptomes of HER2-CA-expressing cells experiencing a soft ECM or depleted of YAP/TAZ closely matched each other (lanes 3 and 4); in turn, these cells displayed a gene expression

Fig. 3 | Oncogenes empower a disproportional cellular response to ECM mechanical properties to drive pancreatic tumorigenesis. a, Representative bright-field images and quantifications of *R26-rtTAM2*; *Kras^{G12D}* pancreatic acini embedded in 3D hydrogels. Images are representative of $n=3$ biologically independent experiments. Scale bars, 200 μm. Data are mean + s.d. **b**, qRT-PCRs for the differentiated acinar cell marker amylase (*Amy*) and the ductal/progenitor markers K19 (*Krt19*) and *Sox9* in pancreatic acini, treated as in **a**. Data are presented as mean + s.d. of $n=3$ independent samples. $^{****}P=2.39\times10^{-6}$. Data are normalized to 18S rRNA. **c**, Representative YAP/TAZ immunofluorescence pictures ($n=3$) of pancreatic acini expressing K-Ras^{G12D} and embedded in 0.1 kPa or 0.5 kPa hydrogels, as in **a**. Scale bars, 50 μm. **d**, Representative bright-field and YAP/TAZ immunofluorescence pictures of the indicated pancreatic acini treated with defactinib (Defact.) or Cyto.D. Images are representative of $n=3$ biologically independent experiments. Scale bars, 400 μm (top) and 50 μm (bottom). **e**, Quantifications of the percentage of ADM events in samples treated as in **d**. Data are presented as mean + s.d. of $n=3$ independent samples. $^{****}P=10^{-15}$. See controls in Extended Data Fig. 3f. **f**,**g**, Representative ($n=3$ independent samples) histological stainings, YAP/TAZ immunohistochemical (IHC) images and pMLC immunofluorescence images of the indicated pancreata treated with the LOX inhibitor BAPN (**f**, see scheme of Extended Data Fig. 3g) or with the ROCK inhibitor fasudil (**g**). Genotypes analysed were *Ptf1a-cre^{ERTM}* (WT), *Ptf1a-cre^{ERTM}*; *Kras$^{LSL\text{-}G12D/+}$*(*Kras^{G12D}*) and *Ptf1a-cre^{ERTM}*; *Kras$^{LSL\text{-}G12D/+}$*; *Trp53$^{LSL\text{-}R172H/+}$*(*Kras^{G12D}*; *Trp53^{R172H}*). Scale bars, 100 μm (histological and immunohistochemical stainings) and 19 μm (immunofluorescence). See also Extended Data Fig. 3f–l. *P* values were calculated by Sidak's multiple-comparisons tests (**a**,**b**,**e**).

pattern resembling that of control (non-HER2-CA-expressing) cells (lane 2). Overall, a substantial amount of the genes differentially induced by HER2 in standard tissue culture conditions but not in non-permissive mechanical conditions (0.5 kPa) are YAP/TAZ regulated (68%, $n = 1{,}348$). More than 40% (47% or 41% depending on the siRNA pair targeting YAP/TAZ that was considered) of the entire list of HER2-induced genes ($n = 3{,}183$) are YAP/TAZ dependent, highlighting the relevance of these factors and cell mechanics for RTK–Ras oncogene function (see Supplementary Table 1 and Extended Data Fig. 4i for the main biological processes regulated by RTK–Ras–YAP/TAZ oncogenic mechanosignalling).

Oncogenic mechanosignalling mediated by Rac1. We next explored how activated oncogenes intercept YAP/TAZ mechanotransduction. Mechanical activation of YAP/TAZ has been shown to occur through Hippo-dependent and Hippo-independent mechanisms[4].

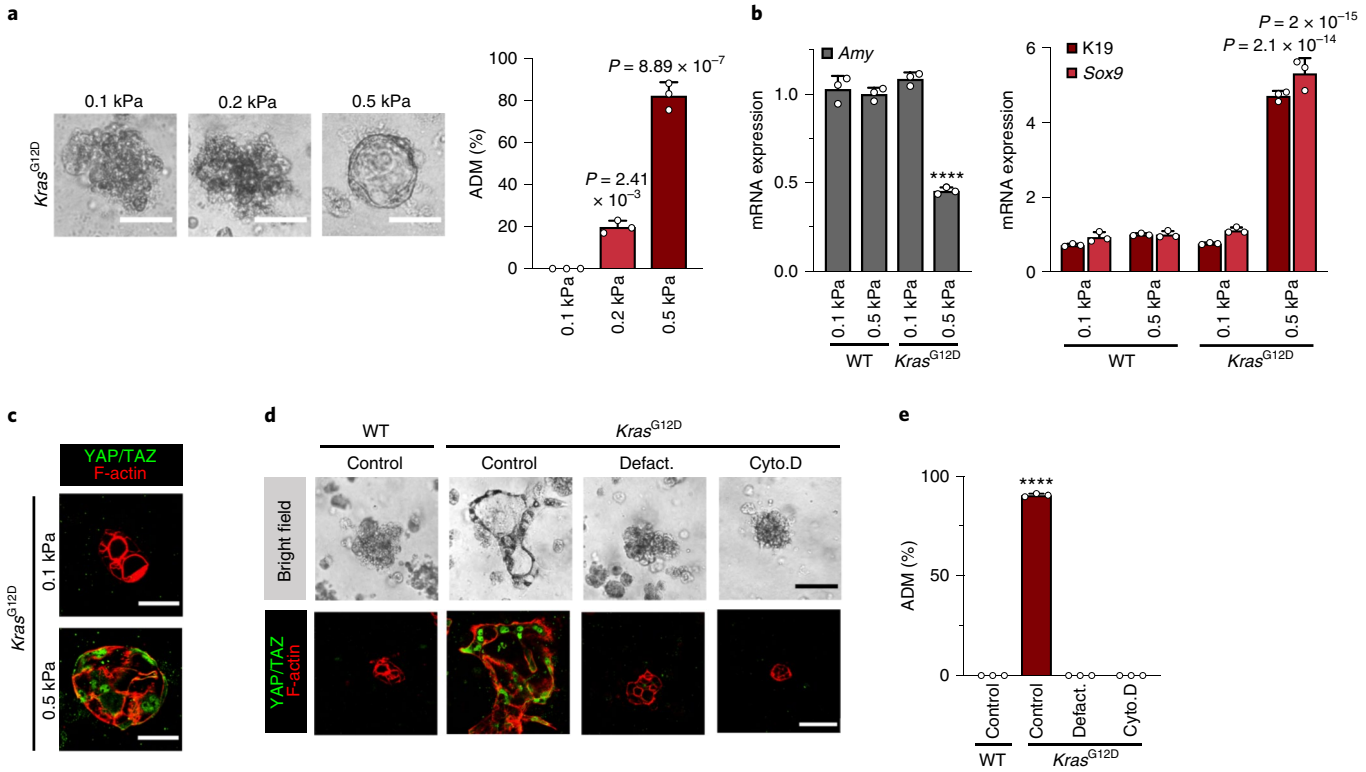

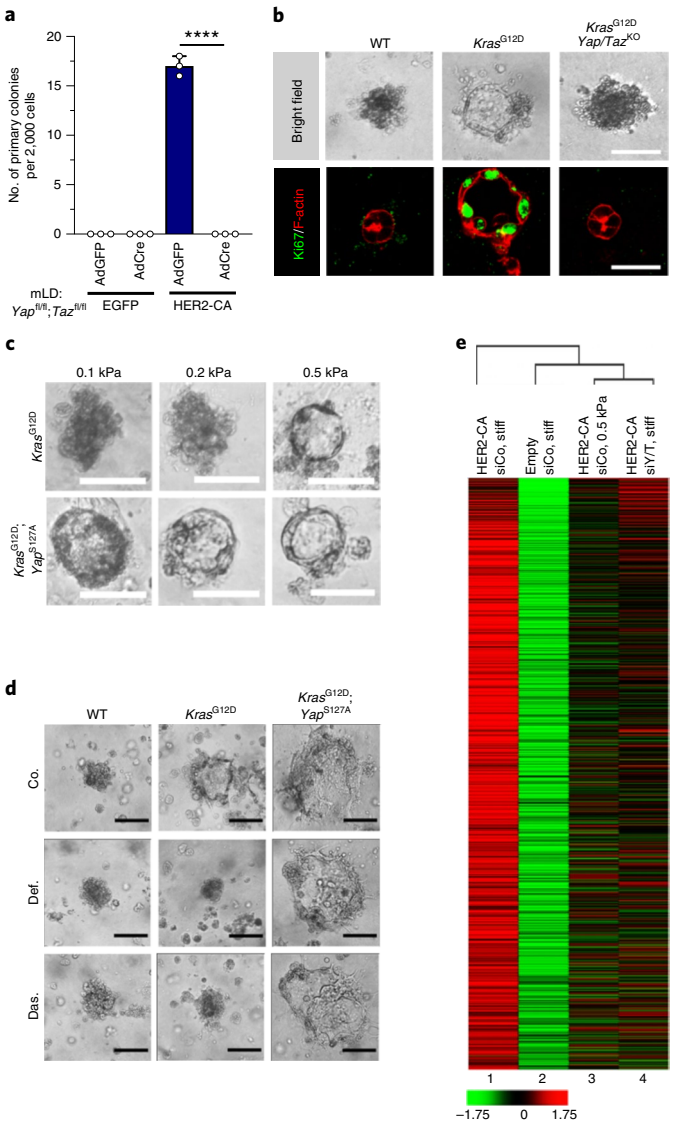

Fig. 4 | YAP and TAZ are the nuclear effectors downstream of cellular changes in mechanical and material properties induced by oncogenes. **a**, Quantifications of the mammary colonies formed by mLD cells derived from $Yap^{fl/fl}$ or $Taz^{fl/fl}$ mice infected with AdCre or AdGFP and transduced with lentiviral constructs expressing EGFP or HER2-CA. Data are mean + s.d. of $n = 3$ biologically independent experiments. $^{****}P = 3.66 \times 10^{-10}$, based on one-way ANOVA with Sidak's multiple-comparisons test. **b**, Representative bright-field and Ki67 immunofluorescence pictures of $Kras^{LSL\text{-}G12D/+}$ ($Kras^{G12D}$) or $Kras^{LSL\text{-}G12D/+}$; $Yap^{fl/fl}$; $Taz^{fl/fl}$ ($Kras^{G12D}$; Yap/Taz^{KO}) pancreatic acini. Images are representative of $n = 6$ biologically independent experiments. Scale bars, 50 µm. See controls in Extended Data Fig. 4d. **c**, Representative bright-field images of *R26-rtTAM2*; $Kras^{G12D}$ ($Kras^{G12D}$) or *R26-rtTAM2*; $Kras^{G12D}$; *tetO-*Yap^{S127A} ($Kras^{G12D}$; Yap^{S127A}) pancreatic acini embedded in 3D hydrogels of increasing stiffness. Images are representative of $n = 3$ biologically independent experiments. Panels show the same set of controls related to Fig. 3a. Scale bars, 200 µm. **d**, Representative bright-field images of wild-type, $Kras^{G12D}$ or $Kras^{G12D}$; Yap^{S127A} pancreatic acini treated with defactinib (Def.), dasatinib (Das.) or control medium (Co.). Images are representative of $n = 3$ biologically independent experiments. Panels show the same set of controls related to Fig. 3d. Scale bars, 400 µm. For **c** and **d**, see controls of YAP expression in Extended Data Fig. 4f and h. **e**, Hierarchical clustering of gene expression profiles from RNA-seq data of control (empty-vector-expressing) MCF10A cells (lane 2); HER2-CA-expressing cells plated on stiff substrates and transfected with control siRNA (siCo, lane 1) or YAP/TAZ siRNAs (siY/T, lane 4); or HER2-CA-expressing cells cultured on 0.5 kPa hydrogels (lane 3). The heatmap shows row-wise standardized expression of genes significantly upregulated (fold change ≥ 1.33, Benjamini–Hochberg false discovery rate (FDR) ≤ 5%) in MCF10A cells by HER2-CA in standard culture conditions. Genes are ordered according to decreasing average expression in HER2-CA-expressing cells plated on stiff substrates (lane 1).

We first excluded the involvement of the Hippo pathway, as the inhibitory phosphorylation of YAP by the large tumour suppressor (LATS) kinases remained unchanged in transformed cells (Extended Data Fig. 5a); then, direct measurement of phosphorylated LATS, identifying the active pool of these kinases, showed that LATS activity remained constitutive, unaltered by oncogenes (Extended Data Fig. 5b). Thus, YAP/TAZ activation by oncogenic mechanosignalling occurs independently from Hippo pathway regulation.

Downstream of RTK–Ras signalling, the Rho family of small GTPases serves as a pivotal regulator of cytoskeletal biology[24]. A body of work in vitro and in vivo suggested Rac1 and Rac1 GEFs as the most promising effector of Ras-induced transformation, but through poorly understood mechanisms[25,26]. We thus hypothesized that, at least in part, oncogenes could modify the cell's material properties and mechanoresponsiveness by hijacking Rac1 and, in so doing, inducing oncogenic reprogramming. Several lines of

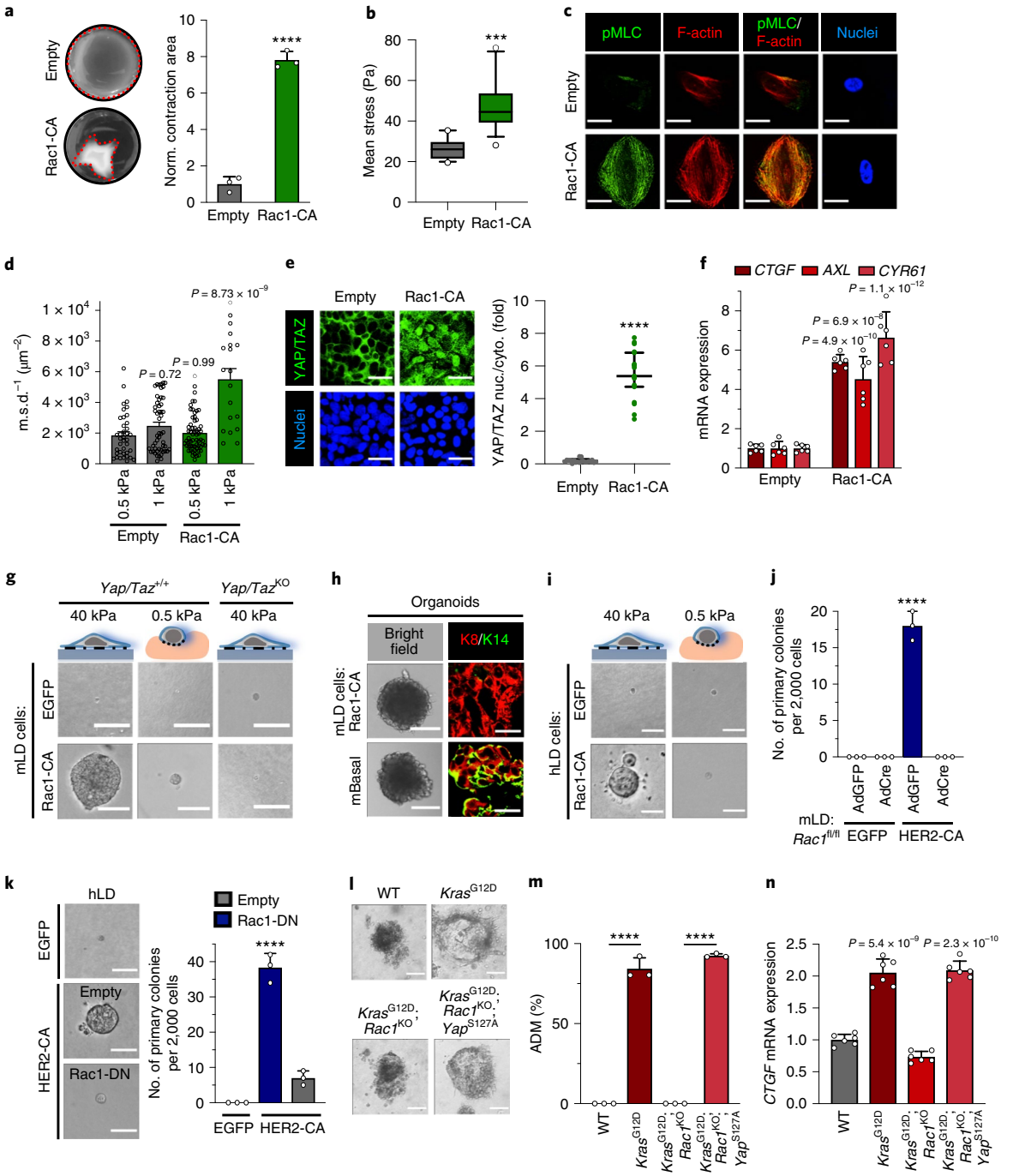

Fig. 5 | Oncogenes modify the cell's mechanical properties through Rac1 activation. a, Collagen contraction assays of Rac1-induced MCF10A cells. Data are mean + s.d. of $n = 3$ independent samples. $^{****}P = 4.56 \times 10^{-5}$. **b**, TFM measurements of MCF10A cells on 3 kPa substrates. Control data (Empty) are the same data as in Fig. 2b. Data are box-and-whiskers plots (whiskers: from 10th to 90th percentile; box: from 25th to 75th percentile; line within the box: median) of $n > 12$ independent samples. $^{***}P$ value $= 2.80 \times 10^{-5}$. **c**, Representative pMLC immunofluorescence images ($n = 3$) of MCF10A cells. Scale bars, 40 μm. **d**, Particle-tracking microrheology of MCF10A cells seeded on 0.5 kPa and 1 kPa hydrogels. Control data (Empty) are the same data as in Fig. 2e. Data are mean + s.d. of $n > 19$ independent samples. **e**, YAP/TAZ localization. Data are mean ± s.d. of $n > 19$. Scale bars, 38 μm. $^{****}P = 10^{-15}$. **f**, qRT-PCRs of YAP/TAZ targets (*CTGF*, *AXL*, *CYR61*) in MCF10A cells seeded on 1 kPa hydrogels. Data are mean + s.d. of $n = 6$ independent samples. Data are normalized to GAPDH. **g**, Representative images ($n = 3$) of *Yap*$^{+/+}$; *Taz*$^{+/+}$ or *Yap*^{KO}; *Taz*^{KO} mLD cells cultured on 40 kPa or 0.5 kPa hydrogels, and then seeded in a clonogenic medium. Scale bars, 170 μm. **h**, Representative bright-field and immunofluorescence images ($n = 3$) of Rac1-CA-expressing mLD organoids and mBasal organoids, as in Fig. 1e. Scale bars, 400 μm (left) and 17 μm (right). **i**, Representative images ($n = 3$) of hLD cells and outgrowths on 40 kPa or 0.5 kPa hydrogels. Scale bars, 170 μm. **j**, Quantifications of the colonies formed by *Rac1*$^{fl/fl}$ mLD cells. Data are mean + s.d. of $n = 3$ independent experiments. $^{****}P = 1.14 \times 10^{-7}$. **k**, Representative images ($n = 3$) and quantifications of colonies formed by hLD cells expressing Rac1-DN. Scale bars, 170 μm. Data are mean + s.d. of $n = 3$ independent samples. $^{****}P = 1.84 \times 10^{-5}$. **l**,**m**, Representative bright-field images ($n = 3$) (**l**) and quantifications (**m**) of ADM events of pancreatic acini of the indicated genotypes (see Methods). Scale bars, 70 μm. Data are mean + s.d. of $n = 3$ independent experiments. $^{****}P = 5.25 \times 10^{-9}$. **n**, qRT-PCRs of the YAP/TAZ endogenous target *Ctgf* in pancreatic acini treated as in **l**. Data are presented as mean + s.d. of $n = 6$ independent samples. Data are normalized to 18S rRNA. See also Extended Data Fig. 5k,l. *P* values were calculated by the unpaired two-sided *t*-test (**a**,**b**,**e**) and by one-way ANOVA with Sidak's multiple-comparisons test (**d**,**f**,**j**,**k**,**m**,**n**).

evidence support this prediction. First, we discovered that a constitutively active version of Rac1 (Rac1-CA, that is, the GTP-bound form) phenocopied the effects of HER2-CA or oncogenic K-Ras, leading to a massive increase in cellular contractility, cell stiffening and YAP/TAZ activation (Fig. 5a–f and Extended Data Fig. 5c–e). Of note, Rac1-induced cell contractility was blunted by ROCK inhibitors (fasudil and Y27632), highlighting a previously underappreciated positive connection between Rac1 and ROCK for the induction of contractility in epithelial cells (Extended Data Fig. 5f).

We next tested the role of Rac1 in oncogene-induced mechanosignalling and cell reprogramming by gain- and loss-of-function assays. By gain of function, Rac1-CA reprogrammed freshly explanted and FACS-purified mouse and human LD cells into cells able to form colonies and self-renewing organoids (Fig. 5g–i and Extended Data Fig. 5g–i) that were closely reminiscent of those induced by HER2 expression. Cell reprogramming occurred only when cells were seeded on rigid substrates (plastic or rigid hydrogels), whereas Rac1-CA was inconsequential in LD cells experiencing a hydrogel of physiological compliance (Fig. 5g,i and Extended Data Fig. 5g,i). The reprogramming ability of Rac1 activation was completely dependent on YAP/TAZ (Fig. 5g and Extended Data Fig. 5g), indicating, along with the above results, that Rac1 acts upstream of YAP.

To validate the role of Rac1 by loss of function, we inactivated Rac1 in HER2-CA-transduced primary cells using independent experimental set-ups, that is, ex vivo AdCre genetic ablation of Rac1 in LD cells from *Rac1*$^{fl/fl}$ mice, or expression of a widely used dominant-negative (DN)-Rac1 mutant (Rac1N17) in human LD cells. As shown in Fig. 5j,k, loss of Rac1 activity by either procedure abolished the effects of HER2. Furthermore, Rac1 was required downstream of oncogenes to promote YAP/TAZ activity (Extended Data Fig. 5j). Extending the functional requirement of Rac1 for oncogene-induced mechanosignalling to pancreatic cells, we employed two strategies, one based on pharmacological inhibition of the Rac-specific GEFs Tiam1 and Trio (NSC23766; Extended Data Fig. 5m), and the other making use of conditional *Rac1*$^{fl/fl}$ alleles (*Rac1*^{KO}; Fig. 5l–n). Consistently, we found that Rac1 was required for ADM downstream of K-Ras. By using cells explanted from doxycycline-inducible *tetO-Yap*^{S127A} transgenic mice, we also found that YAP overexpression could single-handedly rescue oncogene-induced pancreatic cell reprogramming in cells genetically depleted of Rac1 or treated with Rac1 GEF inhibitors (Fig. 5l–n and Extended Data Fig. 5j,k,m). Collectively, this suggests that YAP and TAZ are the nuclear effectors of the RTK–Ras–Rac1 cascade.

Discussion

Here we report that RTK–Ras signalling, a main driver of tumorigenesis, regulates the cell's mechanical properties as an integral element of its ability to reprogram normal cells into tumour-precursor cells. This process leads to the build-up of cytoskeletal tension and cell stiffening, with ensuing activation of YAP/TAZ, whose target genes account for an unexpectedly large fraction of the transcriptional responses downstream of oncogenic signalling. We highlight the role of Rac1 as a mediator of oncogenic mechanosignalling, sufficient and required to empower in primary epithelial cells an enhanced responsiveness to changes in the rigidity of the surrounding ECM. Our findings offer mechanistic support to previous observations connecting YAP activity to Ras-induced tumorigenesis[23,27–29]. Future studies are warranted to explore the contribution of more complex mechanical properties of living tissues and natural ECMs, including viscoelastic behaviours[30,31] (see Supplementary Discussion).

The interplay highlighted between a minimal set of genetic and environmental changes that are required to initiate tumour emergence holds a number of implications for tumour biology. The data suggest that the high compliance (that is, softness) of normal epithelial organs represents an overarching tumour-suppression system at the tissue level. In an extreme interpretation, one may envision that even prototypic oncogenic lesions may not be truly causative, but just permissive, of later tumour-initiating events in the form of altered mechanical properties of the ECM. At the same time, we show that tumorigenic cells can be generated de novo from normal primary cells as soon as these cells express an activated oncogene and are concomitantly allowed to experience supra-physiological mechanical inputs. These findings offer a window of opportunity for tumour prevention. It is tempting to speculate that ECM alterations typical of ageing, inflammation, tissue damage, fibrosis, diabetes and smoking[4] may be associated with an increased rate of tumour emergence due to increased mechanical activation of epithelial cells.

The mechanical framework proposed for tumour initiation may incorporate oncogenic lesions other than those directly involving RTK–Ras signalling. For example, Src, hyperactive in several malignancies, is another oncogene upstream of YAP/TAZ[32]. Another possible example is mutation of p53, whose oncogenic effects have been recently causally linked to the activation of Rho/Rac GTPases, as such controlling cell mechanics and YAP/TAZ activity[32,33].

In hindsight, the crucial role of mechanical signals, here highlighted for primary cells, might also be a general trait of the cell transformation of immortalized cell lines, classically visualized by the induction of clonogenic potential and the by-passing of contact inhibition. These assays have been carried out on tissue culture surfaces (glass or plastic)[34] whose rigidities (in GPa) exceed by many folds the physiological stiffness of real tissues[15], as such raising questions as to what extent the mechanical signal intrinsic to tissue culture conditions may have contributed to the discovery of many oncogenes. When we used immortalized MCF10A cells and monitored their transformation by transduced oncogenes, we found that overexpression of HER2 or K-Ras was inconsequential in cells experiencing adhesion to a physiologically soft hydrogel (0.5 kPa; Extended Data Fig. 6a,b). This at least suggests a link between conventional transformation assays and oncogenic reprogramming of primary cells.

Our findings help solve a conundrum in cancer biology, as YAP and TAZ are broadly activated in most, if not all, solid malignancies, although never directly targeted by activating mutations[35], possibly because unleashing full YAP/TAZ activity may be unachievable solely by mutational events[36–39]. Finding that YAP and TAZ are activated by oncogenic mechanosignalling initiated by the activation of common drivers provides a solution to this conundrum.

Finally, our data may inform research on potential routes to exploit oncogenic mechanosignalling as a vulnerability at the onset of tumorigenesis, including tumour prevention strategies akin to those used by normal tissues to prevent cancer emergence.

Online content

Any methods, additional references, Nature Research reporting summaries, source data, extended data, supplementary information, acknowledgements, peer review information; details of author contributions and competing interests; and statements of data and code availability are available at https://doi.org/10.1038/s41563-020-0615-x.

Received: 20 August 2019; Accepted: 16 January 2020;
Published online: 17 February 2020

References

1. Martincorena, I. et al. Tumor evolution. High burden and pervasive positive selection of somatic mutations in normal human skin. *Science* **348**, 880–886 (2015).
2. Yokoyama, A. et al. Age-related remodelling of oesophageal epithelia by mutated cancer drivers. *Nature* **565**, 312–317 (2019).

3. Lee-Six, H. et al. The landscape of somatic mutation in normal colorectal epithelial cells. *Nature* **574**, 532–537 (2019).
4. Panciera, T., Azzolin, L., Cordenonsi, M. & Piccolo, S. Mechanobiology of YAP and TAZ in physiology and disease. *Nat. Rev. Mol. Cell Biol.* **18**, 758–770 (2017).
5. Humphrey, J. D., Dufresne, E. R. & Schwartz, M. A. Mechanotransduction and extracellular matrix homeostasis. *Nat. Rev. Mol. Cell Biol.* **15**, 802–812 (2014).
6. Northey, J. J., Przybyla, L. & Weaver, V. M. Tissue force programs cell fate and tumor aggression. *Cancer Discov.* **7**, 1224–1237 (2017).
7. Sanchez-Vega, F. et al. Oncogenic signaling pathways in the cancer genome atlas. *Cell* **173**, 321–337 (2018).
8. Van Keymeulen, A. et al. Reactivation of multipotency by oncogenic PIK3CA induces breast tumour heterogeneity. *Nature* **525**, 119–123 (2015).
9. Linnemann, J. R. et al. Quantification of regenerative potential in primary human mammary epithelial cells. *Development* **142**, 3239–3251 (2015).
10. Panciera, T. et al. Induction of expandable tissue-specific stem/progenitor cells through transient expression of YAP/TAZ. *Cell Stem Cell* **19**, 725–737 (2016).
11. Acerbi, I. et al. Human breast cancer invasion and aggression correlates with ECM stiffening and immune cell infiltration. *Integr. Biol.* **7**, 1120–1134 (2015).
12. Levental, K. R. et al. Matrix crosslinking forces tumor progression by enhancing integrin signaling. *Cell* **139**, 891–906 (2009).
13. Paszek, M. J. et al. Tensional homeostasis and the malignant phenotype. *Cancer Cell* **8**, 241–254 (2005).
14. Gauthier, N. C., Masters, T. A. & Sheetz, M. P. Mechanical feedback between membrane tension and dynamics. *Trends Cell Biol.* **22**, 527–535 (2012).
15. Brusatin, G., Panciera, T., Gandin, A., Citron, A. & Piccolo, S. Biomaterials and engineered microenvironments to control YAP/TAZ-dependent cell behaviour. *Nat. Mater.* **17**, 1063–1075 (2018).
16. Parsons, J. T., Horwitz, A. R. & Schwartz, M. A. Cell adhesion: Integrating cytoskeletal dynamics and cellular tension. *Nat. Rev. Mol. Cell Biol.* **11**, 633–643 (2010).
17. Tseng, Y., Kole, T. P. & Wirtz, D. Micromechanical mapping of live cells by multiple-particle-tracking microrheology. *Biophys. J.* **83**, 3162–3176 (2002).
18. Li, S., Balmain, A. & Counter, C. M. A model for RAS mutation patterns in cancers: Finding the sweet spot. *Nat. Rev. Cancer* **18**, 767–777 (2018).
19. Guerra, C. et al. Pancreatitis-induced inflammation contributes to pancreatic cancer by inhibiting oncogene-induced senescence. *Cancer Cell* **19**, 728–739 (2011).
20. Kopp, J. L. et al. Identification of *Sox9*-dependent acinar-to-ductal reprogramming as the principal mechanism for initiation of pancreatic ductal adenocarcinoma. *Cancer Cell* **22**, 737–750 (2012).
21. Burdick, J. A. & Prestwich, G. D. Hyaluronic acid hydrogels for biomedical applications. *Adv. Mater.* **23**, H41–H56 (2011).
22. Zanconato, F. et al. Transcriptional addiction in cancer cells is mediated by YAP/TAZ through BRD4. *Nat. Med.* **24**, 1599–1610 (2018).
23. Gruber, R. et al. YAP1 and TAZ control pancreatic cancer initiation in mice by direct up-regulation of JAK-STAT3 signaling. *Gastroenterology* **151**, 526–539 (2016).
24. Scita, G. et al. Signaling from Ras to Rac and beyond: not just a matter of GEFs. *EMBO J.* **19**, 2393–2398 (2000).
25. Kazanietz, M. G. & Caloca, M. J. The rac GTPase in cancer: from old concepts to new paradigms. *Cancer Res.* **77**, 5445–5451 (2017).
26. Heid, I. et al. Early requirement of Rac1 in a mouse model of pancreatic cancer. *Gastroenterology* **141**, 719–730 (2011).
27. Kapoor, A. et al. Yap1 activation enables bypass of oncogenic Kras addiction in pancreatic cancer. *Cell* **158**, 185–197 (2014).
28. Shao, D. D. et al. KRAS and YAP1 converge to regulate EMT and tumor survival. *Cell* **158**, 171–184 (2014).
29. Zhang, W. et al. Downstream of mutant KRAS, the transcription regulator YAP is essential for neoplastic progression to pancreatic ductal adenocarcinoma. *Sci. Signal.* **7**, ra42 (2014).
30. Vining, K. H. & Mooney, D. J. Mechanical forces direct stem cell behaviour in development and regeneration. *Nat. Rev. Mol. Cell Biol.* **18**, 728–742 (2017).
31. Caliari, S. R. & Burdick, J. A. A practical guide to hydrogels for cell culture. *Nat. Methods* **13**, 405–414 (2016).
32. Sorrentino, G. et al. Metabolic control of YAP and TAZ by the mevalonate pathway. *Nat. Cell Biol.* **16**, 357–366 (2014).
33. Moon, S. H. et al. p53 represses the mevalonate pathway to mediate tumor suppression. *Cell* **176**, 564–580 (2019).
34. Shih, C., Shilo, B. Z., Goldfarb, M. P., Dannenberg, A. & Weinberg, R. A. Passage of phenotypes of chemically transformed cells via transfection of DNA and chromatin. *Proc. Natl Acad. Sci. USA* **76**, 5714–5718 (1979).
35. Zanconato, F., Cordenonsi, M. & Piccolo, S. YAP/TAZ at the roots of cancer. *Cancer Cell* **29**, 783–803 (2016).
36. Aragona, M. et al. A mechanical checkpoint controls multicellular growth through YAP/TAZ regulation by actin-processing factors. *Cell* **154**, 1047–1059 (2013).
37. Chang, L. et al. The SWI/SNF complex is a mechanoregulated inhibitor of YAP and TAZ. *Nature* **563**, 265–269 (2018).
38. Dupont, S. et al. Role of YAP/TAZ in mechanotransduction. *Nature* **474**, 179–183 (2011).
39. Wada, K., Itoga, K., Okano, T., Yonemura, S. & Sasaki, H. Hippo pathway regulation by cell morphology and stress fibers. *Development* **138**, 3907–3914 (2011).

Methods

Plasmids and reagents. pBABEpuro (#1764), pBABE-Puro-KRas*G12V (#46746), pCDNA3-HER2-CA (HER2 V659E) (#16259), FUdeltaGW-rtTA (#19780), FUW-tetO-MCS (#84008), pRRLSIN.cPPT.PGK-GFP.WPRE (#12252), pRK5 beta1 (#16042), pRK5myc RAC1 L61 (Rac1-CA) and pRK5myc Rac1-DN (RAC1 T17N) (#15904) were purchased from Addgene. FUW-tetO-EGFP (#84041) was previously reported[10], and phRG-TK-Renilla was purchased from Promega. CSII-CMV-MCS-IRES-puro was subcloned from CSII-CMV-MCS-IRES-bsd. pBABEpuro-HER2-CA, FUW-tetO-HER2-CA and CSII-CMV-MCS-IRES-HER2-CA were subcloned from pCDNA3-HER2-CA, into pBABEpuro, FUW-tetO-MCS and CSII-CMV-MCS-IRES-puro, respectively. pCS2-KRas*G12V was subcloned from pBABE-KRas*G12V into pCS2+ (ref. [40]). CSII-CMV-MCS-IRES-puro-Itgb1^{V737N} was cloned by PCR mutagenesis from pRK5 beta1 into CSII-CMV-MCS-IRES-puro. CSII-CMV-MCS-IRES-puro-LOXL2 was subcloned from pCMV6-myc-ddk-LOXL2 (Origene #RC200455) into CSII-CMV-MCS-IRES-puro. pBABEpuro-RAC1-CA and FUW-tetO-Rac1-CA were subcloned from pRK5myc RAC1-CA into pBABEpuro and FUW-tetO-MCS, respectively. FUW-tetO-Rac1-DN was subcloned from pRK5myc RAC1-DN into FUW-tetO-MCS. 8xGTIIC–LUX (a synthetic luciferase reporter of YAP/TAZ-dependent transcription) was previously described[38].

Fetal bovine serum (FBS), horse serum (HS), L-glutamine, Pen/Strep (10,000 U ml^{-1}), EMEM, DMEM/F12, DMEM, Waymouth's, Advanced DMEM/F12 medium, trypsin-EDTA 0.05%, ProLong-DAPI, Dispase, insulin-transferrin-selenium-ethanolamine (ITS-X) and bovine pituitary extract (BPE) supplement were from Life Technologies. Acrylamide (AA), bis-acrilamide (BA), ammonium persulfate (APS), tetramethylethylenediamine (TEMED), formaldehyde, Cyto.D, TMSPM, hydrocortisone, cholera toxin, heparin sodium salt, collagenase type I, hyaluronidase, forskolin, soybean trypsin inhibitor (SBTI), dexamethasone, NSC23766, dasatinib, BAPN, tamoxifen, doxycycline hyclate, rat tail collagen I (coating), Phoshatase Inhibitor Cocktail 2, dl-dithiothreitohl and PolyFreeze (OCT) were from Sigma-Aldrich. TriPure Isolation Reagent was from Roche. Matrigel Growth Factor Reduced Basement Membrane Matrix, Phenol Red-Free was from Corning. Rat tail collagen I for 3D culture was from Cultrex. Fibronectin was from Santa Cruz. Recombinant human Noggin, human EGF, human bFGF and murine EGF were from Peprotech. Glycosil, Gelin and Extralink were from ESI Bio. Recombinant human R-spondin-1 was from Sino Biological. Lipofectamine RNAi-MAX, Alexa Fluor 568 Phalloidin and B27 were from Thermo Fisher Scientific. Fasudil and Y27632 were from Tocris Bioscience. TransIT-LT1 was from Mirus Bio. Cre- and GFP-expressing adenoviruses were from University of Iowa, Gene Transfer Vector Core.

Mice. CD-1 mice (IMSR no. CRL:22), BALB/c mice (IMSR no. CRL:28) and NOD-SCID mice (IMSR no. CRL:394) were purchased from Charles River. Transgenic lines used in the experiments were provided by Duojia Pan (*Yap*$^{fl/fl}$), Fernando Camargo (*tetO-Yap*^{S127A}), Guillermina Lozano (*Trp53*$^{LSLR172H/+}$), Tyler Jacks (*Kras*$^{LSLG12D/+}$) and Jens Siveke (*Rac1*$^{fl/fl}$). *Taz*$^{fl/fl}$ and double *Yap*$^{fl/fl}$;*Taz*$^{fl/fl}$ conditional knockout mice were previously described[41]. *Ptf1a-cre*^{ERTM} (IMSR no. JAX:019378) and *R26-rtTAM2* (IMSR no. JAX:006965) mice were purchased from the Jackson Laboratory. Animals were genotyped with standard procedures[42] and with the recommended set of primers. Animal experiments were performed adhering to our institutional guidelines as approved by the animal welfare body (Organismo Preposto al Benessere Animale; OPBA) and authorized by the Ministry of Health.

Cell culture. MCF10A cells were a gift from F. Miller (Karmanos) and were cultured in DMEM/F12 (Gibco) with 5% horse serum, glutamine and antibiotics, freshly supplemented with insulin (Sigma-Aldrich), EGF (Peprotech), hydrocortisone (Sigma-Aldrich) and cholera toxin (Sigma-Aldrich). HEK293 cells were from ATCC and were cultured in DMEM (Gibco) supplemented with 10% FBS, glutamine and antibiotics. HEK293 and MCF10A cells were authenticated by DSMZ/Eurofins Genomics. K-Ras^{G12V}, HER2-CA and Rac1-CA-expressing MCF10A cells were obtained by transduction with retroviral constructs (pBABEpuro-KRas*G12V, pBABEpuro-HER2-CA V659E and pBABEpuro-RAC1-CA); control cells were transduced with empty retroviral constructs (pBABEpuro). C3H10T1/2 fibroblasts were from ATCC and were cultured in EMEM, 10% FBS, glutamine and antibiotics. All cell lines tested negative for mycoplasma contamination. To exclude any toxic effect associated with drug treatments performed throughout, the maximal dose (dasatinib, 100 nM; defactinib, 5 μM; fasudil, 10 μM; Cyto.D, 200 nM; BAPN, 500 μM; Y27632 50 μM) was administered to MCF10A cells for 24 h and viability was assessed with a CellTiter-Glo Luminescent Cell Viability assay (Promega), according to the manufacturer instructions; treatment with a high dose of puromycin (20 ng μl^{-1}) was used as a comparison.

Human mammary tissue. Discard tissue was collected from anonymized healthy women undergoing reduction mastoplasty surgery with informed consent according to our institutional guidelines and the Azienda Ospedaliera di Padova Ethics Committee (CESC).

2D mechanical challenge. For the mechanical challenge of MCF10A cells, cells were plated on standard fibronectin-coated tissue culture dishes or on fibronectin-coated hydrogels of the indicated stiffness (kPa), produced as described previously[38]. Hydrogel formulations in AA, BA, TEMED and APS were as follows: 4% w./v. AA, 0.03% w./v. BA, 1:1,000 v./v. TEMED and 0.1% w./v. APS (0.5 kPa); 4% w./v. AA, 0.06% w./v. BA, 1:1,000 v./v. TEMED and 0.1% w./v. APS (1 kPa); 4% w./v. AA, 0.1% w./v. BA, 1:1,000 v./v. TEMED and 0.1% w./v. APS (2 kPa); 5% w./v. AA, 0.15% w./v. BA, 1:1,000 v./v. TEMED and 0.2% w./v. APS (4 kPa); and 8% w./v. AA, 0.48% w./v. BA, 1:1,000 v./v. TEMED and 0.2% w./v. APS (40 kPa). Cells (4×10^4 cells per cm^2) were seeded in a drop of complete culture medium on top of fibronectin-coated hydrogels; after attachment, the hydrogel-containing wells were filled with the appropriate culture medium. Cells were collected for immunofluorescence or RNA extraction after 24 h or were trypsinized and recovered after 48 h for soft agar assays. For the mechanical challenging of primary murine and human mammary luminal cells, cells were plated on tissue culture dishes coated with collagen I or on hydrogels of the indicated stiffness coated with collagen I in a drop of complete culture medium (see below for details).

Rheological measurements of polyacrylamide (PAA) hydrogels were performed to verify that the hydrogel compositions fitted a purely elastic behaviour with a negligible contribution of the loss modulus (Extended Data Fig. 7). Rheology was carried out using rotating parallel plates at room temperature (Dynamic Stress Rheometer DSR, Rheometrics). The hydrogels (24 mm diameter, 1 mm height) were bonded between two coverslips and measured after swelling overnight. Storage (G') and loss (G'') moduli were calculated as a function of the frequency (from 0.01 to 1.259 Hz) in a constant-strain mode. Young's modulus E was calculated from the elastic shear modulus, $E = 3G$, on the basis of rubber elasticity theory.

Preparation of synthetic hyaluronan and gelatin-based 3D hydrogels. The 3D mechanically defined hydrogels were designed as previously reported[43], with minor modifications. Briefly, under sterile conditions, thiolate HA (Glycosil, ESI Bio), thiolate gelatin (Gelin, ESI Bio) and polyethylene glycol diacrylate (PEGDA; Extralink, ESI Bio) were dissolved in degassed water according to the manufacturer's directions. For the preparation of the hydrogels of defined stiffness for the subcutaneous injections, stock concentrations of 10 mg ml^{-1} Glycosil, 10 mg ml^{-1} Gelin and 5 mg ml^{-1} Extralink and concentrated stocks of ×2 Glycosil and ×5 Extralink were prepared. Solutions were prepared at 1:5 ratios of Extralink/(Glycosil + Gelin) for soft (0.5 kPa) hydrogels and ×5 Extralink/(×2 Glycosil + Gelin) for stiff (9 kPa) hydrogels. For the preparation of hydrogels with a defined stiffness gradient for pancreatic acinar cultures, we prepared stock concentrations of 10 mg ml^{-1} Glycosil and 10 mg ml^{-1} Gelin and three different stock concentrations of Extralink: 4 mg ml^{-1}, 3 mg ml^{-1} and 2 mg ml^{-1} for stiff (0.5 kPa), medium (0.2 kPa) and soft (0.1 kPa) hydrogels, respectively. Solutions were prepared at 1:5 ratios of Extralink/(Glycosil + Gelin).

Murine mammary luminal cell isolation and culturing. Primary mammary cells were isolated from the mammary glands of 8- to 12-week-old virgin CD-1 mice (experiments of Fig. 1a,b,d,f,h and Extended Data Fig. 1b,e,g,i), BALB/c (experiments of Fig. 1i and Extended Data Fig. 1j–n), *Yap*$^{fl/fl}$;*Taz*$^{fl/fl}$ mice (experiments of Fig. 4a and Fig. 5g) or *Rac1*$^{fl/fl}$ mice (experiments of Fig. 5j), as previously described[44]. Briefly, mammary glands were minced and digested before sorting. To separate various subpopulations, cells were stained for 30 min at 4 °C with antibodies against CD49f (BD Biosciences no. 551129), CD29 (BioLegend no. 102222), CD61 (BD Biosciences no. 553347), EpCAM (BioLegend no. 118208) and lineage markers (BD Biosciences no. 558074) in DMEM/F12. The stained cells were then resuspended in PBS/BSA, 0.1% and sorted on a BD FACS Aria sorter (BD Biosciences) into LD cells, LP cells and basal cells. The identity of the sorted populations was confirmed by qRT-PCR for lineage-specific markers (Extended Data Fig. 1b). After FACS purification, cells were seeded in 24-well plates coated with collagen I or on PAA hydrogels and cultured in mouse mammary epithelial growth medium (MMGM: DMEM/F12 supplemented with glutamine, antibiotics, 10 ng ml^{-1} murine EGF, 10 ng ml^{-1} murine bFGF and 4 μg ml^{-1} heparin with 2% FBS). Cells were infected with lentiviral vectors (virus suspension was mixed 1:1 with medium). For primary mammary cell reprogramming, LD or LP cells were transduced for 48 h with FUW-tetO-HER2-CA or FUW-tetO-Rac1-CA in combination with rtTA-encoding lentiviruses (FudeltaGW-rtTA). As a (negative) control, LD cells were transduced with EGFP-expressing vector (FUW-tetO-EGFP) in combination with rtTA-encoding lentiviruses. For the experiments depicted in Fig. 4a and Fig. 5g,j, LD cells were transduced for 24 h with lentiviral vectors as described above and subsequently transduced for 24 hr with either AdCre or AdGFP, as a control. For the experiments depicted in Extended Data Fig. 1n, LD cells were transduced for 48 h with lentiviral vectors encoding for HER2-CA (CSII-CMV-MCS-IRES-HER2^{V659E}), with a self-clustering Integrinβ1 mutant[13] (CSII-CMV-MCS-IRES-puro-Itgb1^{V737N}), or with the empty vector as a control (CSII-CMV-MCS-IRES-puro). After infection, adherent cells were washed and treated with 2 μg ml^{-1} doxycycline for 7 d in MMGM for activating tetracycline-inducible gene expression. After 1 week, mammary cells were detached with trypsin and seeded at a density of 2,000 cells per well in 24-well ultralow attachment plates (Corning) in mammary clonogenic suspension medium (DMEM/F12 containing glutamine, antibiotics, 5% Matrigel, 5% FBS, 10 ng ml^{-1} murine EGF, 20 ng ml^{-1} murine bFGF and 4 μg ml^{-1} heparin) containing doxycycline (2 μg ml^{-1}). Primary colonies were counted 14 d after seeding. To show the self-renewal capacity of

primary colonies, these were recovered from the clonogenic medium by collecting and incubating cell suspensions with an excess volume of ice cold HBSS in order to solubilize Matrigel. After 1 h, colonies were rinsed three times in cold HBSS by centrifugation at 1,000 r.p.m. for 5 min and incubated in trypsin, 0.05% for 30 min to obtain a single-cell suspension. Cells were counted and re-seeded at 2,000 cells per well in 24-well ultralow attachment plates in mammary clonogenic suspension medium. For mammary organoid formation, primary colonies were recovered from clonogenic medium in cold HBSS and transferred in 100% Matrigel. After Matrigel formed a gel at 37 °C, organoid medium was added (Advanced DMEM/F12 supplemented with HEPES, GlutaMAX, antibiotics, B27 ×1, 50 ng ml^{-1} murine EGF, 20 ng ml^{-1} murine bFGF, 4 µg ml^{-1} heparin, 100 ng ml^{-1} Noggin and 1 µg ml^{-1} R-Spondin1) containing doxycycline (2 µg ml^{-1}). Two weeks after seeding, organoids were removed from Matrigel, trypsin-dissociated and transferred to fresh Matrigel. Passages were performed in a 1:4–1:8 split ratio every 2 weeks. For analysis, organoids were recovered from Matrigel and embedded in OCT medium (PolyFreeze, Sigma-Aldrich) to obtain frozen sections for immunofluorescence.

Cleared mammary fat pad transplantation of murine mammary cells. Mammary fat pad transplantations were performed as previously described[10], with minor modifications. Briefly, HER2-CA-expressing mammary organoids (derived from LD cells) were transduced by spinfection with lentiviral vectors encoding for a self-clustering Integrinβ1 mutant[13] (CSII-CMV-MCS-IRES-puro-Itgb1^{V737N}), or with an empty vector as a control (CSII-CMV-MCS-IRES-puro), all in combination (1:1 ratio) with EGFP-encoding lentiviruses (pRRLSIN.cPPT.PGK-GFP.WPRE) for cell tracing. After infection, organoids were transferred in 100% Matrigel and cultured in organoid medium containing doxycycline (2 µg ml^{-1}) for 7 d. HER2-CA/Integrinβ1^{V737N}-expressing organoids were resuspended in 50 µl PBS/10% Matrigel; HER2-CA- and empty-vector-expressing organoids were resuspended in 50 µl PBS/10% Matrigel either alone or in combination with C3H10T1/2 murine fibroblast transduced with lentiviruses encoding the collagen-cross-linking enzyme LOXL2 (CSII-CMV-MCS-IRES-puro-LOXL2; ref. [12]), or with the empty vector (CSII-CMV-MCS-IRES-puro) as a control. Cellular suspensions were injected into the inguinal mammary fat pads of NOD-SCID mice (Charles River), which had been cleared of endogenous mammary epithelium at 3 weeks of age. Animals were then administered doxycycline in their drinking water for 10–12 weeks. Transplanted mammary fat pads were examined by GFP immunofluorescence on sections from paraffin wax-embedded biopsies.

Human mammary luminal cell isolation and culturing. Single-cell suspensions of primary human mammary cells were generated as previously described[9], with minor modifications. Briefly, the ductal tree was mechanically minced and enzymatically digested in tissue dissociation medium (Advanced DMEM-F12 supplemented with HEPES, 1.5% GlutaMAX, 600 U ml^{-1} collagenase and 200 U ml^{-1} hyaluronidase at 37 °C overnight). Cells were spun down 3 min at 700 r.p.m., and the pellet was further dissociated in 0.25% trypsin-EDTA for 5 min followed by the addition of 5 mg ml^{-1} dispase and 1 µg ml^{-1} DNaseI for a further 10 min. Digestion was stopped in Advanced DMEM 10% FBS, and cells were filtered through a 40 µm strainer to remove residual tissue fragments and cell aggregates. Single-cell suspensions of primary mammary cells were stained with CD31 (BioLegend no. 303119), CD45 (BD Biosciences no. 557833), CD49f (BD Biosciences no. 555736) and EpCAM (BD Biosciences no. 347197) in DMEM for 30 min at 4 °C. After excluding CD31$^+$CD45$^+$(Lin$^+$) cells, mammary cells were sorted into four populations: LD cells, CD49f$^+$EpCAM$^+$; LP cells, CD49f$^+$EpCAM$^+$; basal cells, CD49f$^+$EpCAM$^-$; and stromal cells, CD49f$^-$EpCAM$^-$, using a FACS Aria III (BD Biosciences). The identity of the separated populations was validated by gene expression analysis (see Extended Data Fig. 1d). Freshly isolated primary LD cells were seeded in human mammary epithelial growth medium (HMGM; Advanced DMEM/F12 supplemented with HEPES, GlutaMAX, 0.5% FBS, 4 µl ml^{-1} BPE, 10 ng ml^{-1} hEGF, 10 mM Y27632, 10 mM forskolin and antibiotics). After FACS purification, cells were seeded in 24-well plates coated with collagen I or on PAA hydrogels and transduced with lentiviral vectors (virus suspension was mixed 1:1 with medium). For primary mammary cell reprogramming, LD cells were transduced for 48 h with FU-tetO-HER2-CA or FUW-tetO-Rac1-CA in combination with rtTA-encoding lentiviruses (FudeltaGW-rtTA). As a (negative) control, LD cells were transduced with EGFP-expressing vector (FUW-tetO-EGFP) in combination with rtTA-encoding lentiviruses. For the experiments depicted in Fig. 5k, LD cells were transduced for 48 h with lentiviral vectors encoding for HER2-CA either alone or together with lentiviral vectors encoding for Rac1-DN (FUW-tetO-Rac1-DN), in combination with rtTA-encoding lentiviruses.

After infection, adherent cells were washed and treated with 2 µg ml^{-1} doxycycline for 7 d in HMGM for activating tetracycline-inducible gene expression. After 1 week, mammary cells were detached with trypsin and seeded at a density of 2,000 cells per well in 24-well ultralow attachment plates (Corning) in mammary clonogenic suspension medium (Advanced DMEM/F12 containing HEPES, GlutaMAX, antibiotics, 5% Matrigel, 2% FBS, 10 ng ml^{-1} human EGF, 4 µl ml^{-1} BPE, 10 mM forskolin and 2 µg ml^{-1} doxycycline). Primary colonies were counted 14 d after seeding. To show the self-renewal capacity of primary colonies, these were recovered from the clonogenic medium by collecting and incubating cell suspensions with an excess volume of ice cold HBSS in order to solubilize Matrigel. After 1 h, colonies were rinsed three times in cold HBSS by centrifugation at 1,000 r.p.m. for 5 min and incubated in 0.05% trypsin for 30 min to obtain a single-cell suspension. Cells were counted and re-seeded at 2,000 cells per well in 24-well ultralow attachment plates in mammary clonogenic suspension medium.

Subcutaneous injection of primary human mammary cells. Human luminal cells, isolated and cultured as described above, were transduced with lentiviral vectors encoding for HER2-CA (CSII-CMV-MCS-IRES-HER2-CA) or with the empty vector (CSII-CMV-MCS-IRES-puro) as a (negative) control. All cells were co-transduced with EGFP-encoding lentiviruses (pRRLSIN.cPPT.PGK-GFP.WPRE) for in vivo cell tracing. After 1 week, mammary cells were trypsinized and embedded in stiff (9 kPa) or soft (0.5 kPa) synthetic hyaluronan- and gelatin-based 3D hydrogels (10^6 cells per 100 µl). Cell suspensions were subcutaneously injected prior to hydrogel gelification into the flank on immunocompromised 4- to 6-week-old NOD/SCID female mice (100 µL for each injection). Tumour masses were removed and fixed in 4% PFA for subsequent analyses 7 weeks after the injection.

3-D collagen contraction assays. Collagen contraction assays were performed as previously described[45], with minor modifications. Briefly, collagen I solution (1.5 mg ml^{-1}) was prepared by neutralizing the pH of acid-solubilized rat tail collagen I (Cultrex) with NaOH and PBS buffer. MCF10A cells (4×10^5 cells per well) were embedded in neutralized collagen (300 µl per well) in 24-well ultralow attachment plates, the collagen hydrogel was polymerized at 37 °C for 40 min and culture medium was added on top. For the experiments in Extended Data Fig. 2a, conditioned medium (CM) was added to the collagen gels. CMs were obtained from the post-confluent culture of MCF10A cells transduced with the empty vector or retroviral vectors encoding for HER2-CA or K-Ras^{G12V}. For the experiments in Extended Data Fig. 5f, Rac1-CA-expressing cells or control cells (empty-vector-transduced) were treated for 24 h before embedding in collagen with the following drugs: 10 µM fasudil (ROCK inhibitor, Tocris Biosciences), 5 µM defactinib (FAK inhibitor, Selleckchem), 100 nM dasatinib (Src inhibitor, Sigma-Aldrich), 50 µM Y27632 (ROCK inhibitor, Tocris Biosciences) or DMSO as a control. For the experiments in Extended Data Fig. 2h, MCF10A cells were transfected with siRNAs 24 h before embedding in collagen. After overnight incubation, the extent of contraction was assessed by subtracting the area of the gel from the well area using ImageJ software. Experiments were performed in triplicate at least twice.

Traction force microscopy. Polyacrylamide substrates were prepared as described in the literature[46] by using a combination of acrylamide (4% w./v.) and methylene-bis-acrylamide (0.1% w./v.). Carboxyl-modified fluorescent polystyrene particles (0.50 µm diameter, Life Technologies) were suspended in the polyacrylamide solutions in a volume ratio of 1:100. The substrates were functionalized with fibronectin at a final concentration of 50 µg ml^{-1}. Cells were seeded on polyacrylamide substrates and allowed to adhere for 24 h. Images of cells and fluorescent substrate-embedded beads were acquired by using a wide-field fluorescent microscope (Olympus Cell-R) equipped with a UPLSAPO ×20 objective (numerical aperture, NA = 0.75). Then, cells were detached by trypsinization to capture images of undeformed substrates. Images of fluorescent particles with and without cells were combined into a stack and aligned using the ImageJ plug-in 'align slices in the stack'. Displacement fields were obtained by a custom-written particle image velocimetry (PIV) ImageJ plug-in (http://imagej.net/PIV_analyser). The plug-in performs an iterative algorithm, which recursively calculated the displacement in a smaller region (interrogation window) using information from the previous computations to filter out wrong displacement vectors. The interrogation window size was progressively reduced (128, 64 and 32 pixels with 0.181 µm per pixel) to obtain a better PIV resolution. From the displacement field, Fourier transform traction cytometry (FTTC) was then used to estimate the traction stress by using the FTTC ImageJ plug-in. Average stresses were calculated on a region of interest (ROI) of 174.46×149 µm^2 around each cell.

Multiple-particle-tracking microrheology. Multiple-particle-tracking microrheology was performed as previously described[47], with minor modifications. Carboxyl-modified fluorescent polystyrene particles (0.50 mm diameter, Polyscience) were introduced into adherent cells by using a ballistic gun (Bio-Rad). Helium gas at 2,000 psi was used to force a macro-carrier disk coated with particles to crash into a stopping screen. The force of collision was transferred to the particles, causing their dissociation from the macro-carrier and the bombardment of cells. Once bombarded, cells were extensively washed with PBS and left to recover for 24 h in culture medium. After recovery, cells were seeded (2×10^4 cm^{-2}) on 1 kPa or on 0.5 kPa PAA hydrogels, formulated as above and covalently attached to a fluorodish treated with TMSPM (Sigma-Aldrich) in a 13 µl drop covered with a 2.54 cm^2 Kapton disk (DuPont), in order to obtain a maximal hydrogel height of 120 µm. After 24 h, the motion of the intracellular fluorescent beads was recorded for a total of 6 s at 100 frames per second (yielding a total of 600 frames per video) using a digital camera (Hamamatsu, ORCA-Flash2.8) attached to a personal computer, and CamControl video capture software mounted on an inverted fluorescence microscope (Olympus IX81) equipped with a fluorescent mercury lamp (Olympus U-LH100L-3). A water immersion objective (×60 objective with NA = 1.35) at ×1.6 magnification was used for particle tracking. Videos were kept

short (the total duration was 6 s) to avoid the photo-bleaching of particles. The total number of analysed particles was at least 200 from more than 19 cells and regions for each sample. Particle-tracking microrheology allows the monitoring of local viscoelastic properties of living cells with a high spatio-temporal resolution, collecting and analysing the Brownian motions of particles embedded in the cytoplasm. Once the nanoparticle trajectories had been obtained, the mean squared displacement (m.s.d.) of each at 0.5 s was calculated from the following equation:

$$\langle \Delta r^2(\tau) \rangle = \langle [x(t-\tau) - x(t)]^2 + [y(t-\tau) + y(t)]^2 \rangle$$

where angular brackets mean time average, τ is the time scale and t is the elapsed time.

Primary pancreatic acinar cell isolation and culturing. Primary pancreatic acini were isolated and cultured as previously described[44] from the pancreas of 6- to 9-week-old mice. Explants were seeded in neutralized rat tail collagen type I (Cultrex)/acinar culture medium (1:1), and overlaid with acinar culture medium (Waymouth's medium supplemented with 0.1% FBS, 0.1% BSA, 0.2 mg ml^{-1} SBTI, ×1 ITS-X, 50 µg ml^{-1} BPE, 1 µg ml^{-1} dexamethasone and antibiotics) once the collagen formed a gel. ADM events were assessed 5 d after seeding. To activate K-Ras overexpression and to concomitantly delete *Yap/Taz* or *Rac1* alleles, acinar cells derived from *Kras*$^{LSL\text{-}G12D/+}$; *Yap*$^{fl/fl}$; *Taz*$^{fl/fl}$ or from *Kras*$^{LSL\text{-}G12D/+}$; *Rac1*$^{fl/fl}$ mice were infected with AdCre for 3 h at 37 °C before seeding, or with AdGFP as a (negative) control. To induce YAP^{S127A} expression, acinar cells derived from *R26-rtTAM2*; *tetO-Yap*^{S127A} mice were cultured in the presence of doxycycline (2 µg ml^{-1}).

For the experiment described in Fig. 3d,e, Fig. 4d, Extended Data Fig. 4g,h and Extended Data Fig. 5m, acinar culture medium was supplemented either with the FAK inhibitor defactinib (Selleckchem), 10 µM; with the Src inhibitor dasatinib (Sigma-Aldrich), 100 nM; with Cyto.D (Sigma-Aldrich), 200 nM; with the Rac1-GEF inhibitor NSC23766, 100 µM (Sigma-Aldrich); or with DMSO as a control.

For the experiment described in Figs. 3a–c and 4c, pancreatic acini were embedded in synthetic hyaluronan- and gelatin-based 3D hydrogels and overlaid with acinar culture medium (Waymouth's medium supplemented with 0.1% FBS, 0.1% BSA, 0.2 mg ml^{-1} SBTI, ×1 ITS-X, 50 µg ml^{-1} BPE, 1 µg ml^{-1} dexamethasone and antibiotics) once the hydrogels gellified.

RNA-seq. Cells were harvested by the RNeasy Mini Kit (Qiagen) for total RNA extraction, and contaminant DNA was removed by the RNase-Free DNase Set (Qiagen).

RNA-seq libraries for deep-sequencing were prepared with the Illumina TruSeq Standard Total RNA with Ribo-Zero GOLD kit, and sequencing was performed with Illumina HiSeq2500. About 40 M reads per sample were obtained. Raw reads were aligned using STAR[48] version 2.5.3a to build version hg19 of the human genome. Counts for UCSC annotated genes were calculated from the aligned reads using the featureCounts function of the Rsubread R package[49]. Normalization and differential analysis were carried out using the edgeR package[50] and R (version 3.3.1). Raw counts were normalized to obtain counts per million mapped reads (CPM) and reads per kilobase per million mapped reads (RPKM). Only genes with a CPM greater than 1 in at least one sample were retained for differential analysis. Genes were considered significantly regulated when fold changes were equal or greater than 1.33 for upregulated genes or equal or lower than 0.75 for downregulated genes, with a Benjamini–Hochberg FDR of less than or equal to 5%. Hierarchical clustering was carried out using the Hierarchical Clustering of the MultiExperiment Viewer (MeV 4.8; http://mev.tm4.org) package with a Euclidean distance metric and average linkage clustering, using the row-wise standardized RPKM of genes with a RPKM greater than 1 in siCo-transfected HER2-CA–MCF10A cells plated on stiff substrates that were significantly upregulated compared with the control MCF10A cells on stiff substrates. Gene ontology (GO) analyses were performed using Enrichr[51]. The list of GO terms significantly enriched (P value ≤ 0.05) in HER2-induced genes whose expression is dependent on YAP/TAZ and substrate stiffness is presented in Supplementary Table 1.

K-Ras-driven pancreatic tumorigenesis in vivo. For the induction of recombination in pancreatic acini of adult mice, *Ptf1a-cre*^{ERTM} (control) or mice of the indicated genotypes received three intra-peritoneal injections of 1 mg each of tamoxifen (Sigma-Aldrich) dissolved in corn oil (10 mg ml^{-1}) at 4 weeks of age and were killed after 6 months. For the pharmacologic inhibition of collagen cross-linking, mice were administered with 3 mg ml^{-1} of the lysyl oxidase inhibitor BAPN (Sigma-Aldrich) in their drinking water from 5 weeks of age until death. For the pharmacologic inhibition of intracellular actomyosin contractility, mice received each week four intra-peritoneal injections of 10 mg kg^{-1} of the ROCK inhibitor fasudil (Tocris Bioscience) dissolved in water, from 5 weeks of age until death. All experimental groups treated with BAPN or fasudil were killed at 16 weeks of age, and pancreata were collected for analyses.

Luciferase reporter assays. Luciferase assays were performed in HEK293 cells transfected with the TEAD reporter (8xGTIIC–LUX). The luciferase reporter (25 ng cm^{-2}) was transfected together with phRG-TK-Renilla (25 ng cm^{-2}) to normalize for transfection efficiency. Expression construct doses were the following: HER2-CA, 62.5 ng cm^{-2}; K-Ras^{G12V}, 2.5 ng cm^{-2}; and Rac1-DN, 37.5 ng cm^{-2}. DNA content transfected in all samples was kept uniform by adding a pBluescript plasmid up to 250 ng cm^{-2}. Cells were plated at 40% confluence (day 0), transfected with the indicated siRNAs (day 1) and the following day (day 2) transfected with DNA. Cells were harvested after 48 h of treatment (day 3). Firefly luciferase activity was measured with an Infinite F200PRO plate reader (Tecan). Data are presented as firefly/*Renilla* luciferase activity.

RNA interference. The siRNA transfections were done with Lipofectamine RNAi-MAX (Thermo Fisher Scientific) in antibiotic-free medium according to the manufacturer's instructions. Sequences of siRNAs are provided in Supplementary Table 2.

qRT-PCR. MCF10A cells were collected using the RNeasy Mini Kit (Qiagen) for total RNA extraction, and contaminant DNA was removed by DNase treatment. Total RNA from pancreatic or mammary primary cells was extracted using TRIzol reagent (Thermo Fisher Scientific). The qRT-PCR analyses were carried out on reverse-transcribed cDNAs with QuantStudio 5 (Applied Biosystems, Thermo Fisher Scientific) and analysed with QuantStudio Design and Analysis software (version 1.4.3). Expression levels are always normalized to *GAPDH*, or to *18-S rRNA* for experiments with primary pancreatic cells. PCR oligonucleotide sequences are listed Supplementary Table 3.

Western blots. Immunoblots were carried out as previously described[52]. Primary antibodies used were anti-YAP/TAZ (Santa Cruz Biotechnology, sc-101199), anti-P-YAP (Cell Signaling Technology, 4911), anti-LATS (Cell Signaling Technology, 3477), anti-p-LATS (Cell Signaling Technology, 8654) and anti-GAPDH (Millipore, MAB374). Uncropped immunoblots are presented in Supplementary Fig. 1.

Immunofluorescence. Immunofluorescence on PFA-fixed cells and on PFA-fixed paraffin wax-embedded tissue slices was performed as previously described[10]. Primary antibodies were YAP/TAZ (Santa Cruz Biotechnology no. sc-101199), Ki67 (Spring Bioscience no. M3062), phospho-MLC (Cell Signaling Technology no. 3671, for staining on fixed cells, or no. 3675, for staining on paraffin wax sections), FAK (Millipore no. 06-543), phospho-FAK (BD Biosciences no. 611722), vinculin (Sigma-Aldrich no. V9264), paxillin (Abcam no. ab32084), K8 (Abcam no. ab14053), K14 (Abcam no. ab7800) and GFP (Abcam no. ab13970). F-actin was stained with Alexa Fluor 568 Phalloidin (Thermo Fisher Scientific). Secondary antibodies (1:200) were from Molecular Probes. Samples were counterstained with ProLong-DAPI (Molecular Probes, Life Technologies) to label cell nuclei. Confocal images were obtained with a Leica TCS SP5 equipped with a CCD camera and analysed using Volocity software (PerkinElmer, version 5.5.1). For immunofluorescence on mammary organoids, outgrowths freshly recovered from Matrigel were embedded in OCT tissue-freezing medium (PolyFreeze, Sigma-Aldrich) and frozen on dry ice. Cryostat sections of 8 µm were cut at –20 °C. Sections were mounted on glass slides and dried for at least 30 min. The sections were then fixed with 4% formaldehyde for 10 min. After washing with PBS, the sections were processed as previously described[10]. For immunofluorescence on pancreatic primary cells, pancreatic cells were fixed overnight in PBS + 4% PFA at 4 °C, permeabilized with two washes in PBS + 0.5% NP40 for 20 min at 4 °C and followed by one wash in PBS + 0.3% Triton X-100 for 20 min at room temperature. After two washes in PBS + 0.1% Triton X-100 (PBST) for 15 min at room temperature, cells were blocked with two washes in PBST + 10% goat serum (GS) for 1 h at room temperature and incubated overnight with primary antibodies. The following day, cells were washed twice in PBST + 2% GS for 15 min at 4 °C and five more times in PBST + 2% GS for 1 h at 4 °C. Secondary antibodies were incubated overnight. The third day, cells were washed five times in PBST for 15 min, incubated 20 min with DAPI solution and mounted in glycerol. For immunofluorescence on mammary, lung tissue and subcutaneous tumour masses, biopsies were fixed with PFA, paraffin wax embedded and cut in 10-µm-thick sections. Sections were rehydrated, and antigen retrieval was performed by incubation in citrate buffer (0.01 M sodium citrate dihydrate, 0.05% Tween, pH 6) at 95 °C for 20 min. Slides were then permeabilized (10 min at room temperature with PBS + 0.3% Triton X-100) and processed as described above. Cytoskeletal features (average number of FAs and amount of pMLC staining per cell) and YAP/TAZ nuclear versus cytoplasmic ratios were quantified by using NIH ImageJ analysis software with the same threshold in each stain. Immunohistochemical staining experiments were performed on PFA-fixed, paraffin wax-embedded tissue sections as previously described[52]. For immunohistochemistry the antibodies used were anti-YAP (Proteintech Group no. 13584-1-AP) and anti-TAZ (Sigma-Aldrich no. HPA007415).

Picrosirius red collagen staining. Collagen visualization on PFA-fixed, paraffin wax-embedded tissue sections was carried out by picrosirius red staining. Briefly, sections were dewaxed with the following incubation steps: 10 min in 100% xylene, 10 min in 1:1 v./v. xylene/ethanol, 10 min in 100% ethanol and 5 min in 1:1 v./v. ethanol/distilled water. Nuclei were stained in Weigert's iron hematoxylin (Sigma, HT1079) according to the manufacturer's instructions; sections were washed for

10 min in running tap water, and collagen was stained in picrosirius red solution (0.5 g of Direct Red 80 (Sigma, 365548) into 500 ml of 1.3% picric acid solution (Sigma, P6744)) for 1 h. Following the collagen staining, sections were washed twice in acidified water (1:200 v./v. glacial acetic acid) and dehydrated in 100% ethanol, cleared in xylene and mounted with Eukitt quick-hardening mounting medium (Sigma, 03989). Bright-field images and collagen birefringence[53] images were collected with a Leica 5000B microscope under parallel and orthogonal polarized light, respectively, and quantified using ImageJ software; the signal threshold was maintained equal for all images across all conditions.

In situ proximity ligation assay (PLA). In situ PLAs were performed with Duolink In Situ Detection Reagents (Sigma-Aldrich). MCF10A cells were plated on fibronectin-coated glass chamber slides. After 24 h, after cells reached confluency, cells were fixed in 4% PFA for 10 min at room temperature and subjected to PLA, following the manufacturer's instructions. Primary antibodies used in the PLA were anti-TEF1 (BD Biosciences, 610923) and anti-YAP (Proteintech, 13584-1-AP). Images were acquired with a Leica TCS SP5 confocal microscope equipped with a CCD camera and analysed using Volocity software (PerkinElmer, version 5.5.1).

Lenti- and retrovirus preparation. Lentiviral particles were prepared as previously described[52]. Briefly, HEK293T (ATCC) cells were transiently transfected with lentiviral vectors (10 µg per 60-cm^2 dish) together with packaging vectors pMD2-VSVG (2.5 µg) and pPAX2 (7.5 µg) using TransIT-LT1 (Mirus Bio) according to the manufacturer's instructions.

Retroviral particles were prepared as previously described[52]. Briefly, GP2-293 (Takara) cells were transiently transfected with retroviral vectors (15 µg per 60-cm^2 dish) together with pMD2-Env (5 µg per 60-cm^2 dish) using TransIT-LT1. Infections were carried out as previously described[52].

Agar colony formation assay. For the experiments in Extended Data Fig. 6a, MCF10A cells (4×10^4 cm^{-2}) were seeded on 2D hydrogels of the indicated stiffness, or on fibronectin-coated cell culture plastic dishes, and then embedded in agar 48 h later. For the experiments in Extended Data Fig. 6b, MCF10A cells (4×10^4 cm^{-2}) were transfected with the indicated siRNAs and embedded in agar after 48 h. Effective YAP/TAZ downregulation was assessed by immunoblotting. Clonogenic assays were performed as previously described[22]; briefly, MCF10A cells ($0.5–1\times10^3$) were resuspended in complete growth medium with 0.3% agarose (Invitrogen) and were layered onto 0.6% agar beds in six-well plates. Complete medium was added on top of the cells and was replaced with fresh medium twice a week for 3 weeks.

Statistics. The number of biological and technical replicates and the number of animals are indicated in the figure legends, Main text and Methods section. All tested animals were included. The animal ages and sexes are specified in the text and Methods section. The sample size was not predetermined. Randomization was not applicable to our experiments with cell lines. The Student's *t*-test and ANOVA analyses were performed, as indicated in the captions of the figures and supplementary figures, with GraphPad Prism 8.0.2 for Mac software.

Reporting Summary. Further information on research design is available in the Nature Research Reporting Summary linked to this article.

Data availability

The data supporting the findings of this study are available from the corresponding authors on reasonable request. All relevant data used to generate Figs. 1–5 and Extended Data Figs. 1–7 are included in the paper as Source Data. RNA-seq data from this study have been deposited in the GEO database under accession number GSE128037.

References

40. Azzolin, L. et al. Role of TAZ as mediator of Wnt signaling. *Cell* **151**, 1443–1456 (2012).
41. Azzolin, L. et al. YAP/TAZ incorporation in the beta-catenin destruction complex orchestrates the Wnt response. *Cell* **158**, 157–170 (2014).
42. Morsut, L. et al. Negative control of Smad activity by ectodermin/Tif1gamma patterns the mammalian embryo. *Development* **137**, 2571–2578 (2010).
43. Meng, Z. et al. RAP2 mediates mechanoresponses of the Hippo pathway. *Nature* **560**, 655–660 (2018).
44. Panciera, T. et al. De novo generation of somatic stem cells by YAP/TAZ. *J. Vis. Exp.* https://doi.org/10.3791/57462 (2018).
45. Sanz-Moreno, V. et al. ROCK and JAK1 signaling cooperate to control actomyosin contractility in tumor cells and stroma. *Cancer Cell* **20**, 229–245 (2011).
46. Panzetta, V. et al. ECM mechano-sensing regulates cytoskeleton assembly and receptor-mediated endocytosis of nanoparticles. *ACS Biomater. Sci. Eng.* **3**, 1586–1594 (2017).
47. Panzetta, V. et al. Mechanical phenotyping of cells and extracellular matrix as grade and stage markers of lung tumor tissues. *Acta Biomater.* **57**, 334–341 (2017).
48. Dobin, A. et al. STAR: ultrafast universal RNA-seq aligner. *Bioinformatics* **29**, 15–21 (2013).
49. Liao, Y., Smyth, G. K. & Shi, W. featureCounts: an efficient general purpose program for assigning sequence reads to genomic features. *Bioinformatics* **30**, 923–930 (2014).
50. Robinson, M. D., McCarthy, D. J. & Smyth, G. K. edgeR: a Bioconductor package for differential expression analysis of digital gene expression data. *Bioinformatics* **26**, 139–140 (2010).
51. Kuleshov, M. V. et al. Enrichr: a comprehensive gene set enrichment analysis web server 2016 update. *Nucleic Acids Res.* **44**, W90–W97 (2016).
52. Cordenonsi, M. et al. The Hippo transducer TAZ confers cancer stem cell-related traits on breast cancer cells. *Cell* **147**, 759–772 (2011).
53. Rittie, L. Method for picrosirius red-polarization detection of collagen fibers in tissue sections. *Methods Mol. Biol.* **1627**, 395–407 (2017).

Acknowledgements

We thank V. Guzzardo for histology; C. Frasson for FACS; M. Ventre and P. Netti for rheology; E. Armato Smaniotto dai Roveri for human bioptic sample procurement; and D. J. Pan, F. Camargo, G. Lozano, T. Jacks and J. Siveke for gifts of mice. A.C. was supported by a CARIPARO PhD fellowship. The research leading to these results has received funding from the following agencies: the European Research Council (ERC) under the European Union's Horizon 2020 research and innovation programme (DENOVOSTEM grant agreement No. 670126) to S.P.; Fondazione AIRC under the 5 per Mille 2019 programme (ID No. 22759) to S.P.; the Italian Ministry of Education, University and Research (MIUR), MIUR-FARE (No. R16SXW55W4) to S.P. and PRIN 2017 grants to T.P. (No. 2017L8FWY8_004) and S.P. (No. 2017HWTP2K_001); Fondazione CARIPARO, under the CARIPARO Starting Grant programme (No. C94I19001680001) to T.P. and a CARIPARO Ricerca Scientifica di Eccellenza 2018 grant (No. 52008 - 2019.0356) to S.P.; and University of Padua PRID grant to S.P. and L.A. (No. CPDA135844).

Author contributions

T.P. and A.C. performed all in vitro and in vivo experiments. A.R. helped with mammary gland transplantation. T.P and D.D.B. performed human mammary gland experiments; S.G., G.Br. and A.G. performed hydrogel preparation; L.A. performed mouse genetics; M.F., M.C. and S.B. performed bioinformatic analysis; V.P. and S.F. performed microrheology and TFM; M.F. performed histology and histopathological evaluations; and V.V., F.B., M.F. and A.P.D.T. managed human samples. T.P., M.C. and S.P. conceived the initial hypothesis and experimental design, and planned, discussed and organized the work. T.P., A.C., M.C. and S.P. wrote the manuscript.

Competing interests

The authors declare no competing interests.

Additional information

Extended data is available for this paper at https://doi.org/10.1038/s41563-020-0615-x.

Supplementary information is available for this paper at https://doi.org/10.1038/s41563-020-0615-x.

Correspondence and requests for materials should be addressed to M.C. or S.P.

Reprints and permissions information is available at www.nature.com/reprints.

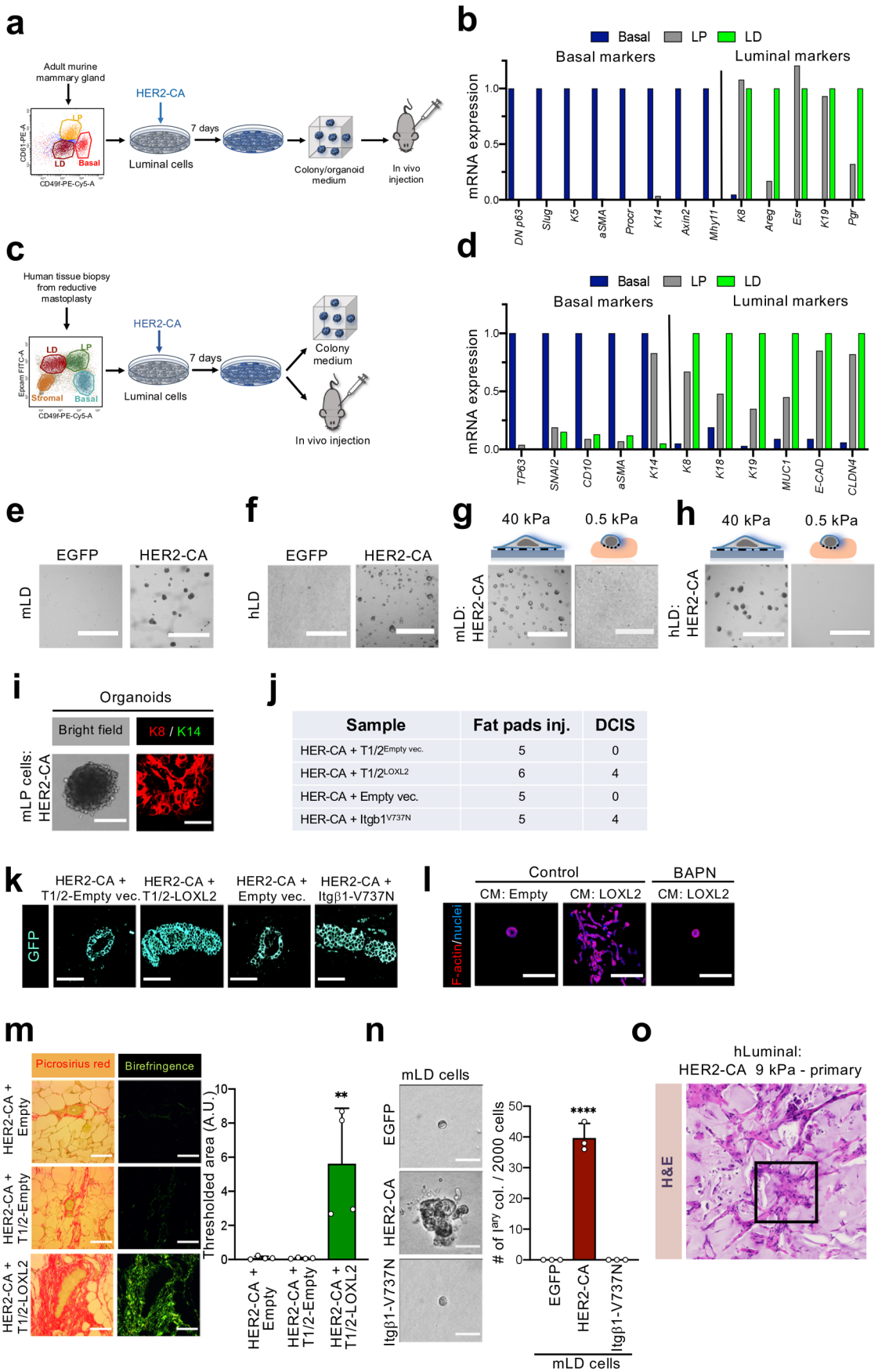

Extended Data Fig. 1 | see figure caption on next page.

Extended Data Fig. 1 | Abnormal substrate rigidity is required for oncogenes to reprogram normal cells into tumorigenic ones. a, Schematic representation of the FACS purification strategy and of the experiments performed with mLD cells. LP: luminal progenitor cells. **b**, qRT-PCR analyses for the indicated basal and luminal mammary cell markers in mBasal, mLP, and mLD cells obtained by FACS, as in Extended Data Fig. 1a. Data are normalized to *Gapdh* and are referred to Basal cells levels for basal genes, and to LD cells levels for all the other luminal markers (each set to 1). Results are representative of n=3 independent experiments (each using mammary glands from n=20 mice) performed with similar results. **c**, Schematic representation of the FACS purification strategy and of the experiments performed with human primary mammary luminal cells. **d**, qRT-PCR analyses for the indicated basal and luminal mammary cell markers in human Basal, LP, and LD cells obtained by FACS, as in Extended Data Fig. 1c. Data are normalized to *GAPDH* and are referred to Basal cells levels for basal genes, and to LD cells levels for all the other luminal markers (each set to 1). Results are representative of n=3 independent experiments performed with similar results. **e–h**, Lower magnification images of experiments shown in Fig. 1a (**e**), in Fig. 1c (**f**), in Fig. 1f (**g**) and in Fig. 1g (**h**). Scale bars, 600 μm. **i**, Representative bright field and immunofluorescence images (n=3 independent experiments) of organoids formed by mLP cells expressing HER2-CA. K14 serves as marker of basal cell identity and K8 serves as marker of luminal cell identity. Scale bars, 400 μm, left and 17 μm, right. **j**, Quantifications of the frequency of different outgrowths emerging from fat pad injection of the same samples of Fig. 1i. Data are representative of n>5 independent samples. **k**, Representative GFP-immunofluorescence pictures (n>5 independent samples) of outgrowths depicted in Fig. 1i, showing that outgrowths emerge form injected mLD cells. Scale bar, 50 μm. **l**, Representative immunofluorescence images (n=3 independent experiments) of *ex-vivo* 3D outgrowths formed by mLD cells expressing HER2-CA, embedded in a collagen-based ECM and treated with conditioned media from Empty-vector (CM: Empty) or LOXL2-transduced C3H10T1/2 fibroblasts (CM: LOXL2). While HER2-expressing cells formed round spheroids/organoids in absence of LOXL2, those embedded in LOXL2-modified collagen formed highly proliferating and invasive outgrowths. This effect relied on LOXL2 enzymatic activity as it was abolished by concomitant treatment with LOX-inhibitor BAPN. Scale bars, 260 μm. **m**, Bright field and birefringence Picrosirius Red images of the same samples shown in Fig. 1i, showing LOXL2 mediated increased fibrillar collagen deposition. Scale bars, 100 μm. Quantifications of total fibrillar collagen by birefringence signal in the same sections are presented as mean + s.d. of n=4 independent samples. ** p-value=$7.13x10^{-3}$. **n**, Representative images and quantifications of colonies formed by mLD cells transduced with the indicated constructs. The expression of the sole integrinβ1 mutant is inconsequential for colony formation by mLD cells. Scale bars, 170 μm. Images and data are representative of n=4 independent experiments. Data are mean + s.d. **** p-value=$4.03x10^{-6}$. **o**, Low magnification of the representative histological staining of the subcutaneous outgrowth shown in Fig. 1j (corresponding to the frame). P-values were calculated by one-way ANOVA with Sidak's multiple comparisons test.

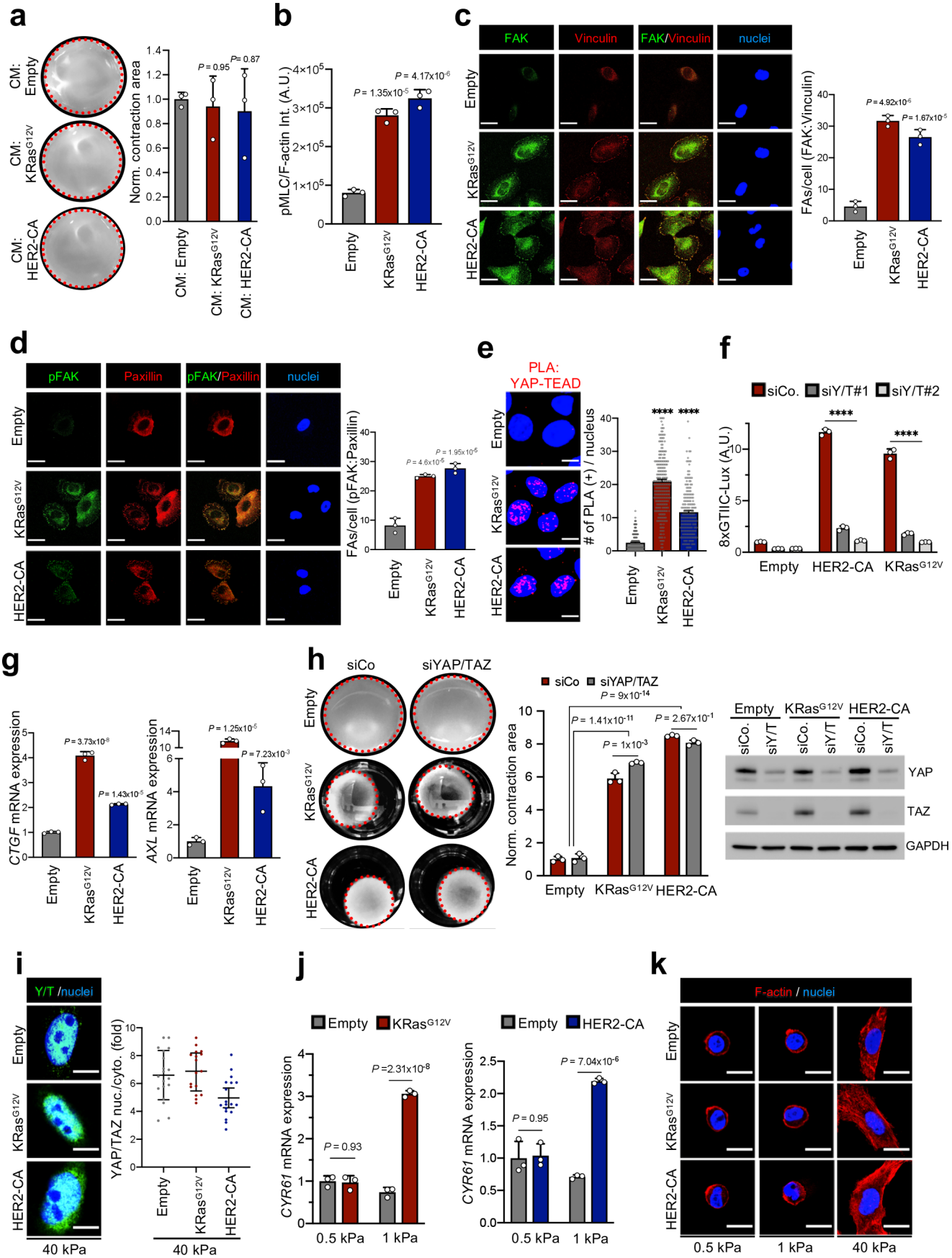

Extended Data Fig. 2 | see figure caption on next page.

Extended Data Fig. 2 | Ras/RTK oncogenes change the mechanical and material properties of cells. a, Representative images and quantifications of collagen contraction assays performed with control MCF10A cells transduced with empty vectors and embedded in 3-D collagen hydrogels with conditioned media obtained from control MCF10A cells (CM: Empty) or cells expressing $Kras^{G12V}$ (CM: $Kras^{G12V}$) or HER2-CA (CM: HER2-CA). Compared with Fig. 2a, this shows that oncogene-mediated cell contractility does not rely on secreted factors. Images and data are representative of n=3 independent samples. Data are mean + s.d. **b**, Quantification of the colocalization of the cytoskeletal stainings for pMLC and F-actin shown in Fig. 2c. Data are as mean + s.d. of n=3 independent samples. **c**, Representative immunofluorescence images and quantifications of FA formation by colocalization of focal adhesion kinase (FAK) and Vinculin in MCF10A cells transduced with HER2-CA or $KRas^{G12V}$. Scale bars, 24 μm. Images and data are representative of n=3 independent experiments. Data are mean + s.d. **d**, Representative immunofluorescence images and quantifications FA maturation by colocalization of phospho-focal adhesion kinase (pFAK) and Paxillin in MCF10A cells transduced with HER2-CA or $KRas^{G12V}$. Scale bars, 24 μm. Images and data are representative of n=3 independent experiments. Data are mean + s.d. **e**, Representative pictures (n=3 independent experiments) and quantifications of proximity ligation assay (PLA) detecting the nuclear interaction between endogenous YAP and endogenous TEAD[37] in control (Empty vector) MCF10A cells or in cells overexpressing $Kras^{G12V}$ or HER2-CA. Scale bars, 9 μm. Data are mean + s.d. of n>200 cells. **** p-value=10^{-15}. **f**, Luciferase assay in post-confluent HEK293 cells transfected with a synthetic reporter for TEAD-dependent transcription (8xGTIIC-Lux) and with the indicated siRNAs and control (Empty) or oncogene-expressing vectors. Data are mean + s.d. of n= 3 independent samples. ****p-value=10^{-15}. **g**, qRT-PCRs of the YAP/TAZ endogenous targets *CTGF* and *AXL*, in MCF10A cells transduced with the indicated oncogene-expressing vectors. Data are mean + s.d. of n= 3 independent samples. **h**, Collagen contraction assays performed with MCF10A cells transduced with the indicated vectors, transfected with control or YAP/TAZ targeted siRNAs, showing that YAP/TAZ are downstream of cell contractility induced by oncogenes. Data are mean + s.d. of n= 3 independent samples. Immunoblots are shown for validation of effective YAP/TAZ depletion. GAPDH serves as loading control. **i**, Representative immunofluorescence images and quantifications of YAP/TAZ localization in MCF10A cells transduced with empty or oncogene-expressing vectors, and seeded on 40 kPa hydrogels. Scale bars, 8 μm. Data are mean +/- s.d. of n>17 independent samples. **j**, qRT-PCRs of the YAP/TAZ endogenous target *CYR61* in MCF10A cells transduced with the indicated vectors and seeded on 0.5 or on 1 kPa hydrogels, as in Fig. 2g. Data are mean + s.d. of n= 3 independent samples. **k**, Representative immunofluorescence images of F-actin of the same MCF10A cells shown in Fig. 2f to visualize cell shape. F-actin was stained with fluorescently-labelled phalloidin and nuclei were counterstained with DAPI. Scale bars, 16 μm. P-values were calculated by unpaired two-sided Student's t-test (**a**), one-way ANOVA with Sidak's multiple comparisons test (**b**–**f**) or two-way ANOVA with Sidak's multiple comparisons test (**g**, **h**, **j**).

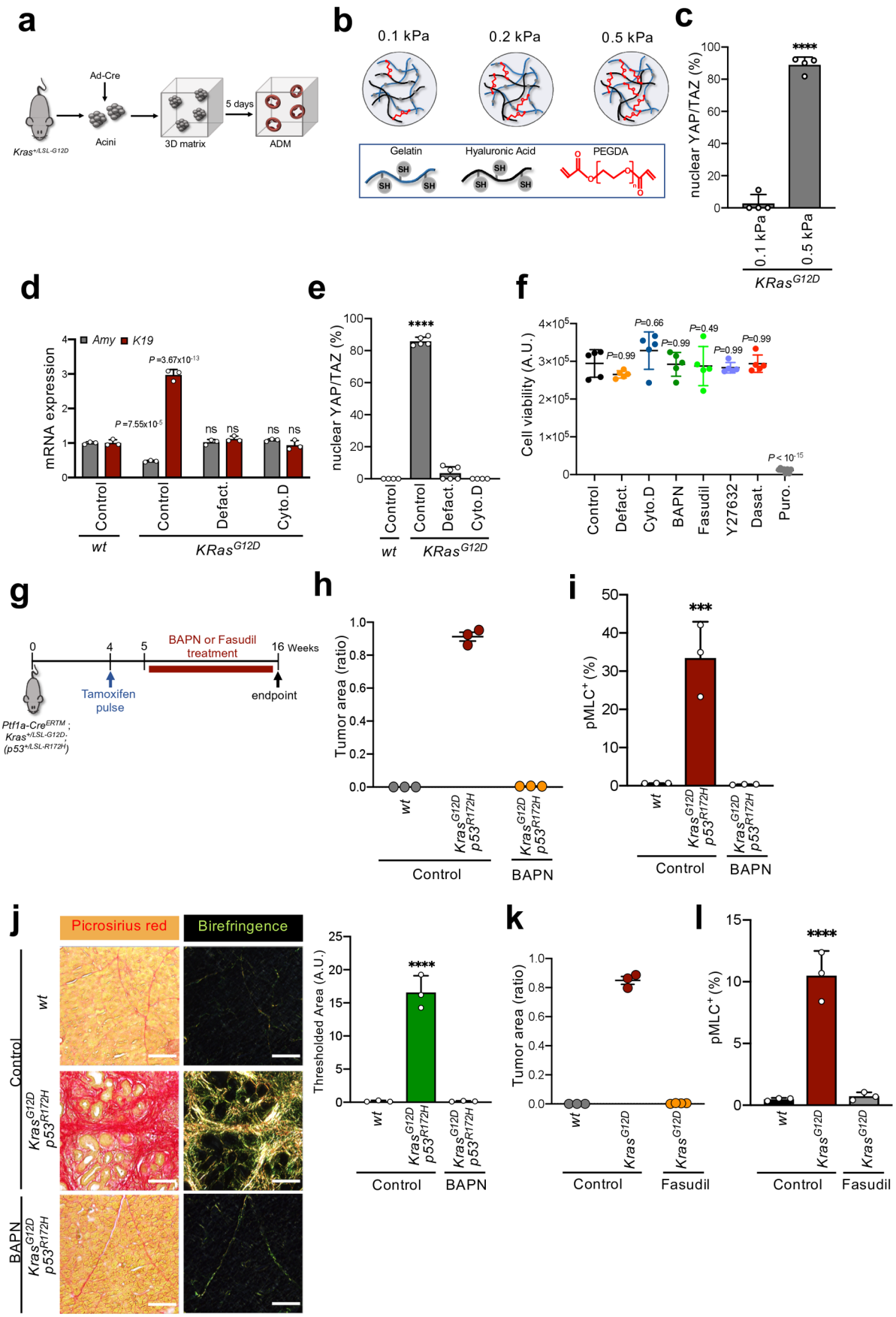

Extended Data Fig. 3 | see figure caption on next page.

Extended Data Fig. 3 | Oncogenes empower a disproportional cellular response to ECM mechanical properties to drive pancreatic tumorigenesis. **a**, Schematic representation of the experimental strategy employed to study pancreatic ADM *ex vivo*. See also methods section for details. **b**, Schematic representation of the chemistry of designer hydrogels employed in the experiments of Fig. 3a–c, Fig. 4c, Extended Data Fig. 3c and Extended Data Fig. 4e, f (see Methods). SH, sulfhydryl group; PEGDA, Poly(ethylene glycol) diacrylate. Hydrogel stiffness was raised by increasing the PEGDA crosslinker concentration, without changing Gelatin and Hyaluronic Acid content. **c**, Quantification of nuclear YAP/TAZ levels in pancreatic acini shown in Fig. 3c. Data mean + s.d. of n=4 independent samples. ****p-value=$4.03x10^{-7}$. **d**, qRT-PCRs assessing the expression levels of the acinar marker *Amylase* (*Amy*) and of the ductal markers *K19* in pancreatic acini of the indicated genotypes, showing that KRas-expressing acini treated with FA or F-actin inhibitors (as in Fig. 3d) remain fully differentiated recapitulating the effects of a soft ECM. Data are mean + s.d. of n= 3 independent experiments. ns, p-value=0.99. Data are normalized to *18-s rRNA*. **e**, Quantification of nuclear YAP/TAZ levels in pancreatic acini shown in Fig. 3d, showing that oncogenic KRas promoted YAP/TAZ activation in a manner opposed by FA and F-actin inhibitors. Data are mean + s.d. of n>4 independent samples. **** p-value=10^{-15}. **f**, Dot-plot depicting cell viability assays comparing MCF10A cells treated with the indicated mechano-inhibitory drugs (at maximal doses, see methods for details) with untreated cells. Drug treatments employed throughout the study do not affect cell viability, at difference with Puromycin (Puro.) treatment, shown as positive control for reduced cell viability. Data are mean +/- s.d. of n=5 independent samples. **g**, Schematic representation of the experimental strategy employed to oppose either ECM stiffness (by BAPN treatment) or intracellular contractility (by Fasudil treatment) at the onset of pancreatic tumorigenesis *in vivo*. **h**, Quantifications of tumor areas in the samples depicted in Fig. 3f. Data are mean +/- s.d. of n=3 independent samples. **i**, Quantifications of pMLC stainings shown in Fig. 3f, showing that BAPN treatment normalized the tensional state of oncogene-expressing pancreatic cells. Data are mean + s.d. of n=3 independent samples. ***p-value=$6.6x10^{-4}$. **j**, Representative bright field and birefringence images of Picrosirius red staining of the same samples shown in Fig. 3f, showing that BAPN treatment inhibited deposition and fibrillar organization of collagen. Quantifications of total fibrillar collagen obtained from birefringence are presented as mean + s.d. of n=3 independent samples. ****p-value=$1.80x10^{-5}$. **k**, Quantifications of tumor areas in the samples depicted in Fig. 3g. Data are mean +/- s.d. **l**, Quantifications of pMLC stainings shown in Fig. 3g. Data are mean + s.d. of n=3 independent samples. ****p-value=$8.88x10^{-5}$. P-values were calculated by unpaired two-sided Student's t-test (**c**) and by one-way ANOVA with Sidak's multiple comparisons test (**d**–**f**, **g**, **i**, **l**).

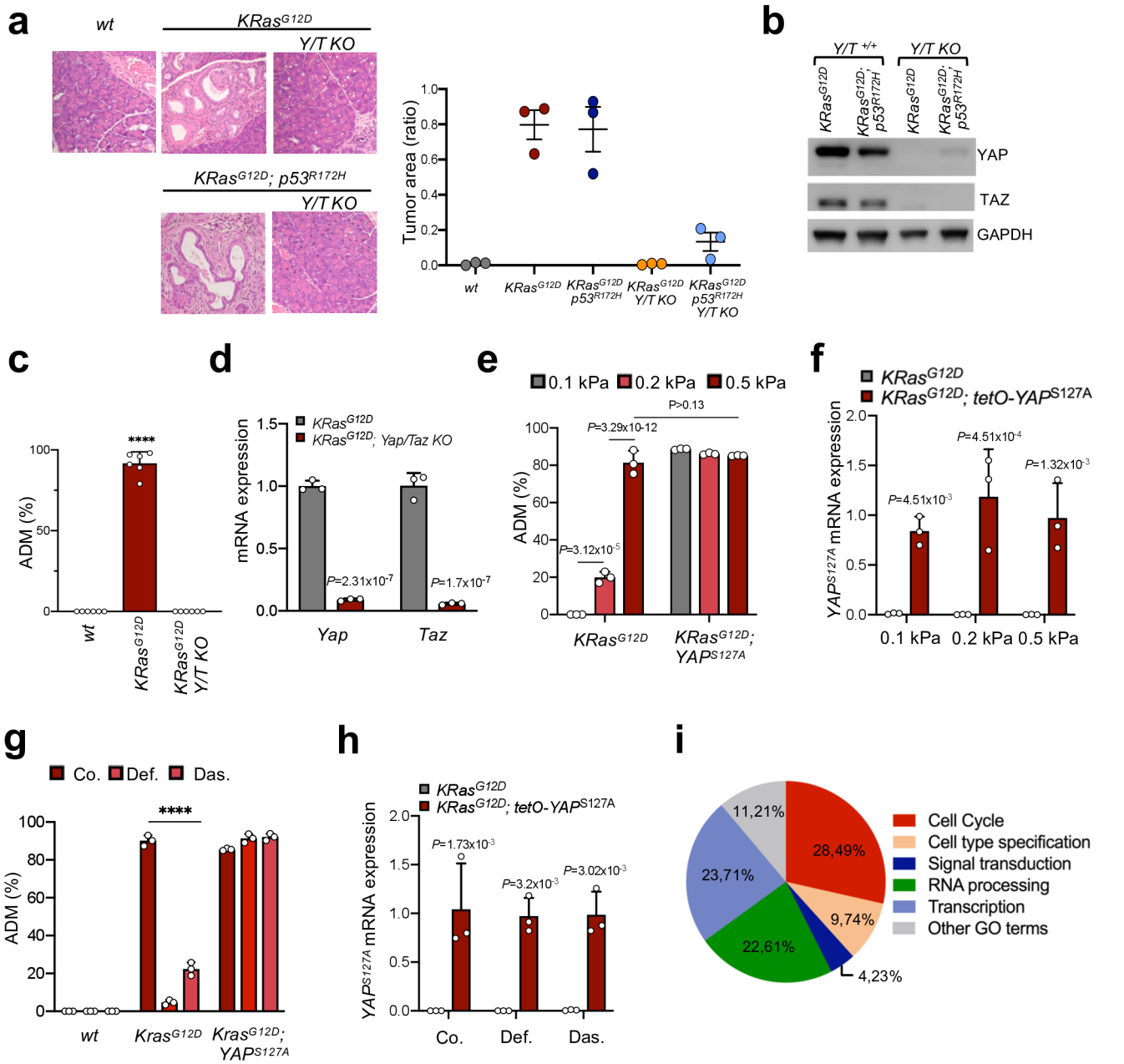

Extended Data Fig. 4 | YAP/TAZ are the nuclear effectors downstream of the changes in the cell's mechanical and material properties induced by oncogenes. a, Representative H&E stainings and quantifications of tumor areas showing that initiation of pancreatic tumorigenesis form acinar cells is dependent on YAP/TAZ. Development of neoplastic lesions was assessed 6 months after tamoxifen administration to mice of the following genotypes: *Ptf1aCre^{ERTM}(wt), Ptf1aCre^{ERTM};KRas$^{+/LSL-G12D}$(KRas^{G12D}), Ptf1aCre^{ERTM};KRas$^{+/LSLG12D}$;Yap$^{fl/fl}$;Taz$^{fl/fl}$ (KRas^{G12D};Y/T KO), Ptf1aCre^{ERTM};KRas$^{+/LSLG12D}$;p53$^{+/LSLR172H}$ (KRas^{G12D};p53^{R172H}), Ptf1a^{CreERTM};KRas$^{+/LSLG12D}$;p53$^{+/LSL-R172H}$;Yap$^{fl/fl}$;Taz$^{fl/fl}$(KRas^{G12D};p53^{R172H};Y/T KO)*. Data are presented as mean +/- s.d. of n=3 independent samples. These experiments are similar to what reported in Ref. [23], although in a different experimental setting, as we tested *Yap/Taz* requirement in absence of experimentally induced pancreatitis. **b**, Immunoblot validating effective *Yap* and *Taz* in vivo knock out in pancreata shown in **a**. GAPDH serves as loading control. Results are representative of n=3 independent experiments. **c**, Quantifications of the percentage of ADM events in pancreatic acini depicted in Fig. 4b. Data are presented as mean + s.d. of n=5 independent samples.****p-value=10^{-15}. **d**, qRT-PCRs validating effective *Yap* and *Taz* ex vivo knock out in pancreatic acini shown in Fig. 4b. Data are presented as mean + s.d. of n=3 independent samples. Data are normalized to *18-s rRNA*. **e**, Quantifications of the percentage of ADM events in pancreatic acini depicted in Fig. 4c. Data are presented as mean + s.d. of n=3 independent samples. **f**, qRT-PCRs validating *YAP^{S127A}* overexpression in pancreatic acini shown in Fig. 4c. Data are mean + s.d. of n=3 independent samples. Data are normalized to *18-s rRNA*. **g**, Quantifications of the percentage of ADM events in pancreatic acini depicted in Fig. 4d. Data are mean + s.d. of n=3 independent samples. ****p-value=10^{-15}. **h**, qRT-PCRs validating *YAP^{S127A}* overexpression in pancreatic acini shown in Fig. 4d. Data are mean + s.d. of n=3 independent samples. Data are normalized to *18-s rRNA*. **i**, Pie chart of the main categories of GO entries associated to the HER2-induced genes that are dependent on YAP/TAZ and substrate stiffness, derived from the RNA-seq of Fig. 4e. Gene Ontology (GO) analysis was performed on the list of HER2-induced genes whose expression is dependent on YAP/TAZ and substrate stiffness (Supplementary Table 1). Of these genes, about 30% are linked to processes related to Cell Cycle progression, whereas others were classified as genes involved in Cell Fate Specification (10%), Signal Transduction (4%), RNA processing (22%) and Transcription (24%). P-values were calculated by unpaired two-sided Student's t-test (**d**), one-way ANOVA with Sidak's multiple comparisons test (**c**, **e**, **f**, **h**) and two-way ANOVA with Sidak's multiple comparisons test (**g**).

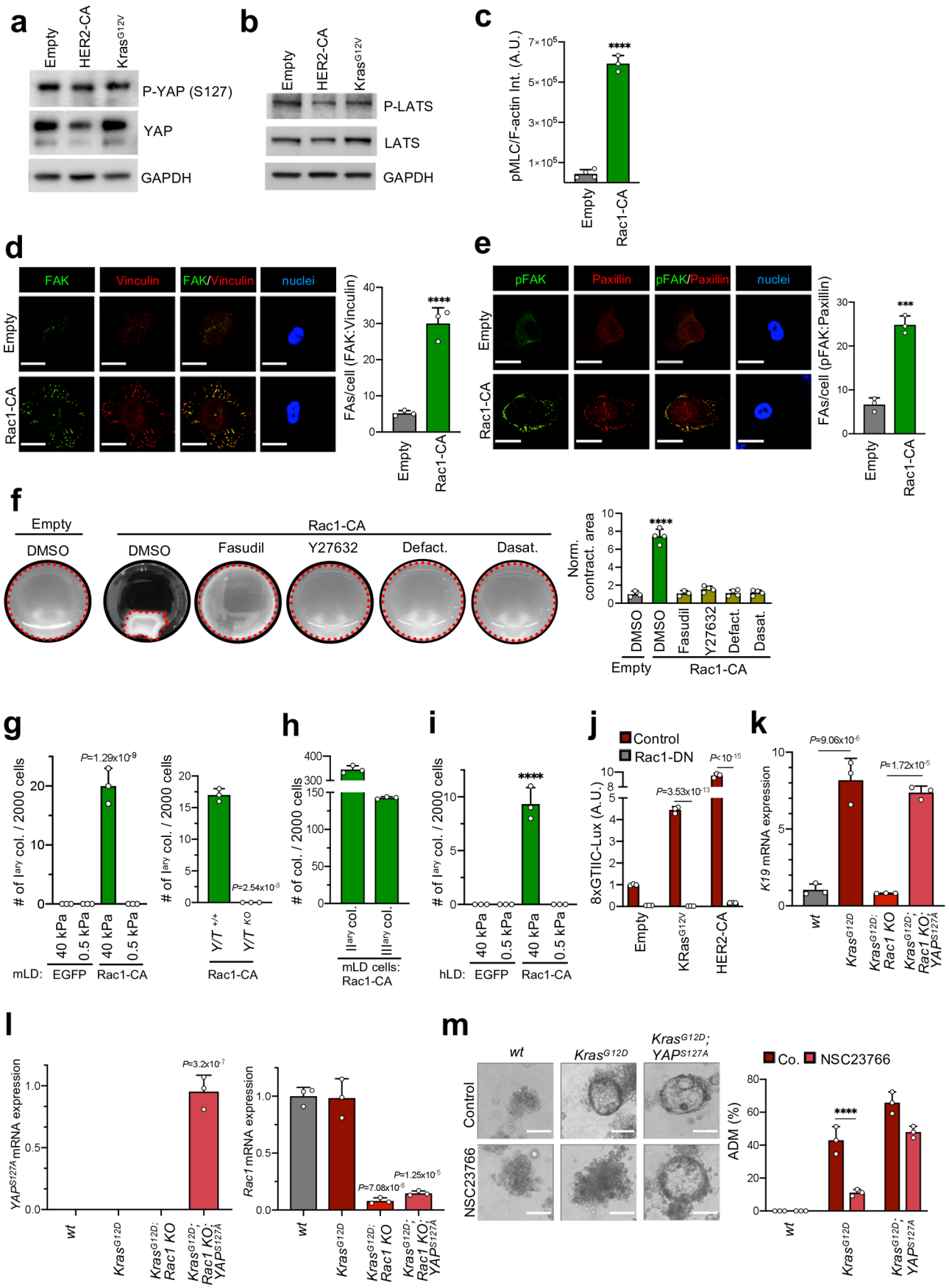

Extended Data Fig. 5 | see figure caption on next page.

Extended Data Fig. 5 | Oncogenes modify the cell's mechanical properties through Rac1 activation. a, Western blots showing that the levels of YAP phosphorylation on the key LATS target residue S127 do not decrease after HER2-CA or $KRas^{G12V}$ expression in MCF10A cells. GAPDH serves as loading control. Phosphorylated vs. total YAP signal ratio (Empty: 1,19; HER2-CA: 1,24; $Kras^{G12V}$: 0,93) was quantified by ImageJ analysis software. Results are representative of n=3 independent experiments, performed with similar results. **b**, Western blots showing that HER2-CA or $KRas^{G12V}$ expression in MCF10A cells does not affect the levels of the active pool of LATS kinases, as assessed by monitoring LATS1-activating phosphorylation on its key residue Thr1079. GAPDH serves as loading control. Phosphorylated vs. total LATS signal ratio (Empty: 1,28; HER2-CA: 1,12; $Kras^{G12V}$: 1,11) was quantified by ImageJ analysis software. Results are representative of n=3 independent experiments, performed with similar results. **c**, Quantification of the colocalization of the cytoskeletal stainings for pMLC and F-actin shown in Fig. 5c. Data are as mean + s.d. of n=3 independent samples. ****p-value=$2.42x10^{-6}$. **d**, Representative immunofluorescence images and quantifications showing that MCF10A cells transduced with Rac1-CA display increased formation of focal adhesion as visualized and quantified by colocalization of focal adhesion kinase (FAK) and Vinculin. Scale bars, 24 μm. Images and data are representative of n=3 independent experiments. Data are mean + s.d. ****p-value=$6.27x10^{-4}$. **e**, Representative immunofluorescence images and quantifications showing that MCF10A cells transduced with Rac1-CA display increased maturation of focal adhesions as visualized and quantified by colocalization of phospho-focal adhesion kinase (pFAK) and Paxillin. Scale bars, 24 μm. Images and data are representative of n=3 independent experiments. Data are mean + s.d. *** p-value=$2.41x10^{-4}$. **f**, Representative images and quantifications of collagen contraction assays performed with MCF10A cells transduced with Rac1-CA and treated with the indicated drugs. MCF10A cells transduced with empty vector are shown as negative control. Data are mean + s.d. of n>3 independent samples. ****p-value=$4.51x10^{-6}$. **g**, Quantifications of the primary mammary colonies formed from $Yap^{+/+};Taz^{+/+}$ or $Yap^{KO};Taz^{KO}$ mLD cells, treated as in Fig. 5g. Data are mean + s.d. of n= 3 independent experiments. **h**, Quantifications of the secondary and tertiary colonies derived from primary colonies formed by Rac1-CA-transduced mLD cells. Data are mean + s.d. of n= 3 independent experiments. **i**, Quantifications of colonies formed by hLD cells treated as in Fig. 5i. Data are mean + s.d. of n= 3 independent experiments. ****p-value=$1.18x10^{-6}$. **j**, Luciferase assay in post-confluent HEK293 cells transfected with 8xGTIIC-Lux, and with empty vector or the indicated oncogene expressing vectors, alone or in combination with vectors coding for Rac1-DN. Data are mean + s.d. of n= 3 independent samples. **k**, qRT-PCRs of the ductal marker *K19* in the pancreatic acini depicted in Fig 5l. Data are mean + s.d. of n=3 independent samples. **l**, qRT-PCRs showing effective YAP^{S127A} overexpression and Rac1 depletion in pancreatic acini depicted in Fig. 5l. Data are presented as mean + s.d. of n=3 independent samples. **m**, Representative bright field images and quantifications of ADM events of pancreatic acini of the indicated genotypes treated with the Rac-specific GEFs Tiam1/Trio inhibitor NSC23766 (100 μM), or left untreated (Control). Images and data are representative of n=3 independent experiments. Scale bars, 70 μm. Data are mean + s.d. **** p-value=3.2x10-5. P-values were calculated by one-way ANOVA with Sidak's multiple comparisons test (**c**–**g**, **i**, **l**, **m**) and two-way ANOVA with Sidak's multiple comparisons test (**j**).

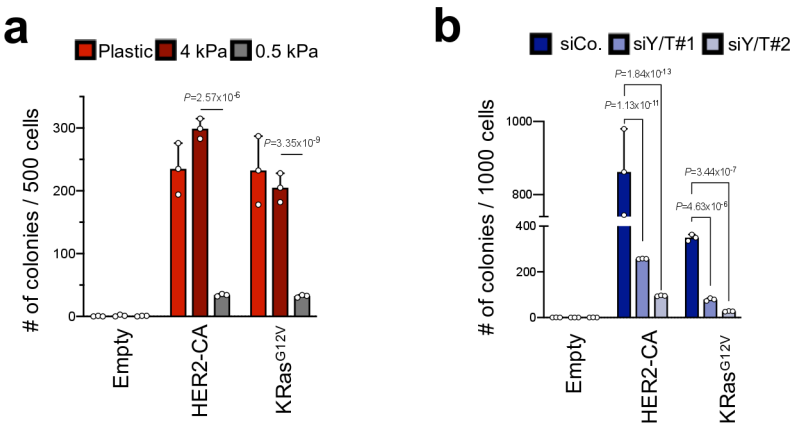

Extended Data Fig. 6 | Transformation of immortalized cells requires sufficient substrate rigidity and YAP/TAZ activity. a, Quantifications of colonies formed by control or oncogene-expressing MCF10A cells, cultured at the three indicated stiffnesses before embedding in agar. Data are mean + s.d. of n=3 independent samples. Controls showing the requirement of YAP/TAZ in similar cell transformation assays are shown in **b**. **b**, Quantifications of colonies formed by control or oncogene-expressing MCF10A cells, transfected with the indicated siRNAs before embedding in agar. YAP/TAZ depletion blunts oncogene-induced cell transformation. Data are mean + s.d. of n=3 independent samples. P-values were calculated by two-way ANOVA with Sidak's multiple comparisons test.

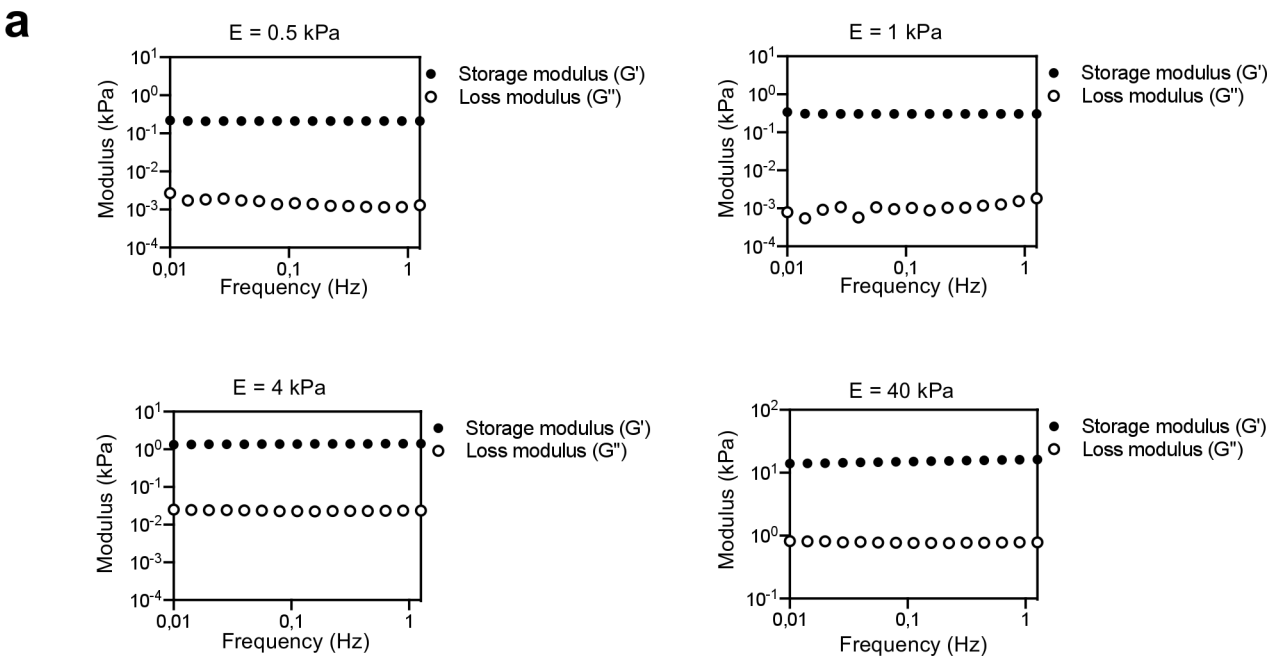

Extended Data Fig. 7 | Rheological measurements validating the purely elastic behavior of PAA hydrogels used in the study. a, Rheological measurements showing Storage (G') and Loss (G'') moduli of PAA hydrogels used in the study as function of the frequency (from 0.01 to 1.259 Hz) in a constant-strain mode. Young's modulus E=3G, is indicated above each panel. Results are representative of n=3 independent experiments, performed with similar results.

nature research

Corresponding author(s): Stefano Piccolo

Last updated by author(s): 31/12/19

Reporting Summary

Nature Research wishes to improve the reproducibility of the work that we publish. This form provides structure for consistency and transparency in reporting. For further information on Nature Research policies, see Authors & Referees and the Editorial Policy Checklist.

Statistics

For all statistical analyses, confirm that the following items are present in the figure legend, table legend, main text, or Methods section.

n/a	Confirmed	
☐	☒	The exact sample size (*n*) for each experimental group/condition, given as a discrete number and unit of measurement
☐	☒	A statement on whether measurements were taken from distinct samples or whether the same sample was measured repeatedly
☐	☒	The statistical test(s) used AND whether they are one- or two-sided *Only common tests should be described solely by name; describe more complex techniques in the Methods section.*
☒	☐	A description of all covariates tested
☒	☐	A description of any assumptions or corrections, such as tests of normality and adjustment for multiple comparisons
☐	☒	A full description of the statistical parameters including central tendency (e.g. means) or other basic estimates (e.g. regression coefficient) AND variation (e.g. standard deviation) or associated estimates of uncertainty (e.g. confidence intervals)
☐	☒	For null hypothesis testing, the test statistic (e.g. *F*, *t*, *r*) with confidence intervals, effect sizes, degrees of freedom and *P* value noted *Give P values as exact values whenever suitable.*
☒	☐	For Bayesian analysis, information on the choice of priors and Markov chain Monte Carlo settings
☒	☐	For hierarchical and complex designs, identification of the appropriate level for tests and full reporting of outcomes
☒	☐	Estimates of effect sizes (e.g. Cohen's *d*, Pearson's *r*), indicating how they were calculated

Our web collection on statistics for biologists contains articles on many of the points above.

Software and code

Policy information about availability of computer code

Data collection	LAS AF 2.7.3.9723 software for Leica TCS SP5 II was used to acquire confocal images. LASV4.4 software was used to acquire pictures of cell cultures with a Leica DM IRB microscope. ImageQuant LAS 4000 1.2 was used to acquire western blot images. QuantStudio Design & Analysis Software v1.4.3 was used to acquire and analyze qPCR data. Wide field fluorescent microscope (Olympus Cell-R) equipped with a UPLSAPO 20× objective was used to acquire traction force microscopy data. An inverted fluorescence microscope (Olympus IX81) equipped with a fluorescent mercury lamp (Olympus U-LH100L- 3) was used to acquire microheology data. Dynamic Stress Rheometer (DSR, Rheometrics Inc., New Jersey, USA) was used for rheological measurements of hydrogels. A Leica 5000B microscope was used to acquire Picrosirius red birefringence images. Hamamatsu NDP scan (version 3.1) software was used to aquire histological and immunohistochemical staining pictures
Data analysis	Volocity 5.5.1 was used for image analysis. GraphPad Prism 8.0.2 for Mac was used for statistical analysis. QuantStudio Design & Analysis Software v1.4.3 was used to acquire and analyze qPCR data. ImageJ v 1.52a software (http://rsbweb.nih.gov/ij/) was used for collagen contraction analysis, for qauntifications of traction force microscopy analyses and for quantifications of collagen birefringence, of immunoflurescence signals and of immunoblot bands. STAR software (Dobin et al., 2013), version 2.5.3a was used to align RNA-seq reads, Rsubread R package 2.0 (Liao et al., 2014), edgeR package 2.3 (Robinson et al., 2010) and R (version 3.3.1) were used to analyse RNA-seq data. MCL package of the Multiple Experiment Viewer (MeV, version 4.1) software was used for unsupervised hierarchical clustering. Enrichr (2016 update) (https://amp.pharm.mssm.edu/Enrichr/) was used for Gene Ontology analyses. PIV analyser (1.1.2) and FTTC Plugin (2015/2/7 update) for ImageJ were used for Traction force microscopy

For manuscripts utilizing custom algorithms or software that are central to the research but not yet described in published literature, software must be made available to editors/reviewers. We strongly encourage code deposition in a community repository (e.g. GitHub). See the Nature Research guidelines for submitting code & software for further information.

Data

Policy information about availability of data

All manuscripts must include a data availability statement. This statement should provide the following information, where applicable:

- Accession codes, unique identifiers, or web links for publicly available datasets
- A list of figures that have associated raw data
- A description of any restrictions on data availability

All RNA-seq data from this study have been deposited in the GEO database under accession number GSE128037.

Field-specific reporting

Please select the one below that is the best fit for your research. If you are not sure, read the appropriate sections before making your selection.

☒ Life sciences ☐ Behavioural & social sciences ☐ Ecological, evolutionary & environmental sciences

For a reference copy of the document with all sections, see nature.com/documents/nr-reporting-summary-flat.pdf

Life sciences study design

All studies must disclose on these points even when the disclosure is negative.

Sample size	No statistical methods were used to predetermine sample sizes, which were based on work in similarly published research. The sample size chosen were sufficient to determine significance in all assays, with reproducible statistical significant difference between conditions in all the experiments. For mouse experiments, differences between genotypes and treatment were so unambigous and consistent that in the spirit of the 3 R's of animal research we reduced the total number of animals as indicated in Figures.
Data exclusions	No data were excluded.
Replication	The number of biological and technical replicates and the number of animals are indicated in Fig. legends, main text and methods. All attempts at replication were successful.
Randomization	Randomization was not applicable for our experiments with cell lines. Mice were randomly allocated to experimental or treatment groups to ensure equal sex/age across genotypes.
Blinding	Investigators were not blinded for analyses relying on unbiased measurements of quantitative parameters, with exception of pathological examination of histological section carried out by a trained pathologists (who was blind to animal genotypes, sex/age or treatment).

Reporting for specific materials, systems and methods

We require information from authors about some types of materials, experimental systems and methods used in many studies. Here, indicate whether each material, system or method listed is relevant to your study. If you are not sure if a list item applies to your research, read the appropriate section before selecting a response.

Materials & experimental systems

n/a	Involved in the study
☐	☒ Antibodies
☐	☒ Eukaryotic cell lines
☒	☐ Palaeontology
☐	☒ Animals and other organisms
☐	☒ Human research participants
☒	☐ Clinical data

Methods

n/a	Involved in the study
☒	☐ ChIP-seq
☐	☒ Flow cytometry
☒	☐ MRI-based neuroimaging

Antibodies

Antibodies used	Primary antibodies used for immunofluorescence stainings were: YAP/TAZ (Santa Cruz Biotechnology Cat# sc-101199), Ki67 (Spring Bioscience Cat# M3062), phospho-MLC (Cell Signaling Technology Cat# 3671), for staining on fixed cells or Cat# 3675, for staining on paraffin sections), FAK (Millipore Cat# 06-543), phospho-FAK (BD Biosciences Cat# 611722), Vinculin (Sigma-Aldrich Cat# V9264), Paxillin (Abcam Cat# ab32084), K8 (Abcam Cat# ab14053), K14 (Abcam Cat# ab7800), GFP (Abcam Cat# ab13970). All primary antibodies were used 1:200. F-actin was stained with Alexa Fluor 568 Phalloidin (Thermo Fisher), 1:200. Secondary antibodies (1:200) were from Molecular Probes (Alexa Fluor® Plus 488,Cat # A32723; Alexa Fluor® Plus 488, Cat # A32795; Alexa Fluor® 568, Cat # A-11011; Alexa Fluor® Plus 647, Cat # A32733). Antibodies used to FACS-sort human mammary gland cells were: CD31 (BioLegend, 303119), CD45 (BD Biosciences, 557833), CD49f (BD Biosciences, 555736), EpCAM (BD Biosciences, 347197). Antibodies used to FACS-sort murine mammary gland cells were: CD49f (BD Biosciences Cat# 551129), CD29

(BioLegend Cat# 102222), CD61 (BD Biosciences Cat# 553347), EpCAM (BioLegend Cat# 118208) and lineage markers (BD Biosciences Cat# 558074). Primary antibodies used for immunoblots were: anti-YAP/TAZ (1:000) (Santa Cruz Biotechnology, sc-101199), anti-P-YAP (1:000) (Cell Signaling Technology, cat. 4911), anti-LATS (1:000) (Cell Signaling Technology, cat. 3477), anti-p-LATS (1:000) (Cell Signaling Technology, cat. 8654) and anti-GAPDH (1:25000) (Millipore, cat. MAB374).

Validation

Primary antibodies for IF against YAP/TAZ (Santa Cruz Biotechnology Cat# sc-101199), K8 (Abcam Cat# ab14053), K14 (Abcam Cat# ab7800) and GFP (Abcam Cat# ab13970) were validated for IF on mouse samples in (Panciera et al., 2016).
The following primary antibodies were validated by the manufacturer:
-Ki67 (Spring Bioscience Cat# M3062) Species Reactivity: Mouse, Applications: immunofluorescence staining. (He et al. Exp Neurol 311:15-32 2019).
Baechler SA et al. Nat Commun 10:83 2019).
-phospho-MLC (Cell Signaling Technology Cat# 3671): Species Reactivity: Human, Applications: Immunofluorescence. (Schipper et al., Nature Communications, 2019; Grego-Bessa et al., Development, 2015)
-phospho-MLC (Cat# 3675): Species Reactivity: Mouse, Applications, Immunofluorescence (Zandi, et al., Cell Reports 2015; Scotcher et al., Nature Communications, 2016).
-FAK (Millipore Cat# 06-543): Species reactivity: Human, Applications: Immunofluorescence (Northey et al., Mol Cell Biol 2008; Yui et al., Cell Stem Cell 2018)
-phospho-FAK (BD Biosciences Cat# 611722) Species reactivity: Human, Applications: Immunofluorescence. (McLean et al., J Biol Chem. 2000)
-Vinculin (Sigma-Aldrich Cat# V9264): Species reactivity: human, Applications: immunofluorescence (Shi M, et al. JBC 287(42), 2012).
-Paxillin (Abcam Cat# ab32084): Species Reactivity: Human; Applications: , immunofluorescence. (Gao et al. J Exp Med 216:688-703, 2019; Nam et al. Biomaterials 200:15-24, 2019).
Antibodies used to FACS-sort human mammary gland cells were validated for FACS in (Linnemann, et al., Development, 2015).
Antibodies used to FACS-sort murine mammary gland cells were validated for FACS in (Panciera et al., 2016).
Primary antibodies for immunoblots were validated by their identification of protein of the correct size, see Supplementary Figure 1.

Eukaryotic cell lines

Policy information about cell lines

Cell line source(s)

MCF10A cells were a gift from F. Miller (Karmanos). HEK293 cells were from ATCC.

Authentication

HEK293 and MCF10A cells were authenticated by DSMZ/Eurofins Genomics. Genetic characteristics were determined by PCR-single-locus-technology. 21 independent PCR-systems Amelogenin, D3S1358, D1S1656, D6S1043, D13S317, Penta E, D16S539, D18S51, D2S1338, CSF1PO, Penta D, TH01, vWA, D21S11, D7S820, D5S818, TPOX, D8S1179, D12S391, D19S433 and FGA were investigated (Promega, PowerPlex 21 PCR Kit).

Mycoplasma contamination

All cell lines tested negative for mycoplasma contamination.

Commonly misidentified lines
(See ICLAC register)

Not present in the study

Animals and other organisms

Policy information about studies involving animals; ARRIVE guidelines recommended for reporting animal research

Laboratory animals

CD-1 mice,BALB/c mice and NOD-SCID mice were purchased from Charles river. Ptf1a-CreERTM and R26-rtTAM2mice were purchased from The Jackson Laboratory. Transgenic lines used in the experiments are described in methods section. 8- to 12-week-old virgin female CD-1 ,BALB/c, Yapfl/fl; Tazfl/fl, Rac1fl/fl and 3-6 weeks old virgin female NOD-SCID mice were used to perform mammary gland experiments. 6- to 9-week-old mice were employed for experiments with pancreatic acini. 6 to 9 weeks old Ptf1aCreERTM(wt), Ptf1aCreERTM;KRas+/LSL-G12D, Ptf1aCreERTM;KRas+/LSLG12D;Yapfl/fl;Tazfl/fl, Ptf1aCreERTM;KRas+/LSLG12D;p53+/LSLR172H, Ptf1aCreERTM;KRas+/LSLG12D;p53+/LSL-R172H;Yapfl/fl;Tazfl/fl mice were employed for in vivo pancreatic tumorigenesis experiments.

Wild animals

No wild animals were used

Field-collected samples

Not present in the study

Ethics oversight

Animal experiments were performed adhering to our institutional guidelines as approved by OPBA and authorized by the Ministry of Health.

Note that full information on the approval of the study protocol must also be provided in the manuscript.

Human research participants

Policy information about studies involving human research participants

Population characteristics	Only female patients of age >18. All included subjects were negative for HIV, HBV, HCV or any other disease related to the study.
Recruitment	Patients undergoing reductive mastoplasty were after signature of informed consent to the donation of bioptic material for the research. Recruited partecipants were informed on the reaserch's scopes and procedures clarifying how participation to the study does not imply nor contemplate any alteration in clinical or surgical protocols. No bias was included in participant recruitment.
Ethics oversight	Discard tissue was collected from anonymized healthy women undergoing reduction mastoplasty surgery with informed consent according to our institutional guidelines and by the Azienda Ospedaliera di Padova Ethics Committee (CESC).

Note that full information on the approval of the study protocol must also be provided in the manuscript.

Flow Cytometry

Plots

Confirm that:

☒ The axis labels state the marker and fluorochrome used (e.g. CD4-FITC).

☒ The axis scales are clearly visible. Include numbers along axes only for bottom left plot of group (a 'group' is an analysis of identical markers).

☒ All plots are contour plots with outliers or pseudocolor plots.

☐ A numerical value for number of cells or percentage (with statistics) is provided.

Methodology

Sample preparation	See Methods sections: "Murine mammary luminal cells isolation and culture" and "Human mammary luminal cells isolation and culture".
Instrument	FACS Aria III (BD Biosciences)
Software	FACS Diva Software
Cell population abundance	No relative abundance of the post-sort fractions was determined. The purity of the populations was experimentally validated by gene expression analyses, as reported in Extended Data Fig. 1.
Gating strategy	The gating strategies are detailed in Methods section and exemplified in Extended Data Fig. 1.

☒ Tick this box to confirm that a figure exemplifying the gating strategy is provided in the Supplementary Information.